© 2019. Published by The Company of Biologists Ltd | Development (2019) 146, dev171207. doi:10.1242/dev.171207

RESEARCH ARTICLE

The transmembrane protein Crb2a regulates cardiomyocyte apicobasal polarity and adhesion in zebrafish

Vanesa Jiménez-Amilburu and Didier Y. R. Stainier*

ABSTRACT

Tissue morphogenesis requires changes in cell-cell adhesion as well as in cell shape and polarity. Cardiac trabeculation is a morphogenetic process essential for forming a functional ventricular wall. Here, we show that zebrafish hearts lacking Crb2a, a component of the Crumbs polarity complex, display compact wall integrity defects and fail to form trabeculae. Crb2a localization is very dynamic at a time when other cardiomyocyte junctional proteins also relocalize. Before the initiation of cardiomyocyte delamination to form the trabecular layer, Crb2a is expressed in all ventricular cardiomyocytes and colocalizes with the junctional protein ZO-1. Subsequently, Crb2a becomes localized all along the apical membrane of compact layer cardiomyocytes and is downregulated in the delaminating cardiomyocytes. We show that blood flow and Nrg/ErbB2 signaling regulate Crb2a localization dynamics. *crb2a*$^{-/-}$ display a multilayered wall with polarized cardiomyocytes: a unique phenotype. Our data further indicate that Crb2a regulates cardiac trabeculation by controlling the localization of tight and adherens junction proteins in cardiomyocytes. Importantly, transplantation data show that Crb2a controls CM behavior in a cell-autonomous manner in the sense that *crb2a*$^{-/-}$ cardiomyocytes transplanted into wild-type animals were always found in the trabecular layer. In summary, our study reveals a crucial role for Crb2a during cardiac development.

KEY WORDS: Cardiac trabeculation, Apicobasal polarity, Crumbs, Junctions, Adhesion

INTRODUCTION

Trabeculation is key to cardiac wall maturation (Sedmera et al., 2000; Liu et al., 2010; Samsa et al., 2013), and defects in this process lead to congenital heart malformations (Jenni et al., 1999; Weiford et al., 2004; Zhang et al., 2013). In zebrafish, prior to trabeculation, cardiomyocytes (CMs) are organized in a monolayer. Complex coordination of different signaling pathways between the endocardium and myocardium, including Nrg/ErbB2 (Gassmann et al., 1995; Lee et al., 1995; Meyer and Birchmeier, 1995; Samsa et al., 2013, 2015; Rasouli and Stainier, 2017) and mechanical forces such as blood flow/contractility (Staudt et al., 2014; Li et al., 2016), promotes the delamination of a subset of CMs that subsequently seed the trabecular layer. Although recent studies have identified regulators of different steps in cardiac development, including trabeculation, much remains unknown.

During tissue morphogenesis, changes in the shape of individual cells, as well as modulation of the actomyosin cytoskeleton and positioning of tight and adherens junction (TJ and AJ, respectively) proteins, translate into changes across the entire tissue (Martin et al., 2010; Gorfinkiel, 2013; Heisenberg and Bellaïche, 2013). Modulation of apicobasal polarity is a fundamental feature of epithelial cells as they undergo proliferation, cell shape changes and migration (Martin-Belmonte and Mostov, 2008; Etienne-Manneville, 2013; Grifoni et al., 2013; Macara and McCaffrey, 2013), and these events also take place during cardiac trabeculation (Staudt et al., 2014; Uribe et al., 2018). Apicobasal polarity complexes, including PAR3/PAR6/aPKC (Kemphues et al., 1988), Scribble/DLG/LGL (Bilder et al., 2000) and crumbs/PALS1/PATJ (Tepass and Knüst, 1990; Tepass, 1996) are known to interact in order to maintain apicobasal identity, cell shape and tissue integrity. A recent study has shown that *Prkci* mouse mutants show trabeculation defects (Passer et al., 2016), further supporting the requirement of apicobasal polarity complexes during cardiac trabeculation. Crumbs (Crb) is a type I transmembrane protein composed of an extracellular domain necessary for homophilic interactions at cell-cell junctions (Letizia et al., 2013; Das and Knüst, 2018), and an intracellular domain required to maintain the identity of the apical domain (Bulgakova and Knüst, 2009). In flies, zebrafish and mammals, mutations in *Crb* affect tissue growth, cytoskeletal rearrangement, junction positioning and stability, as well as the establishment of apicobasal polarity (Grawe et al., 1996; Tepass, 1996; Izaddoost et al., 2002; Omori and Malicki, 2006; Chen et al., 2010; Zou et al., 2012; Alves et al., 2013).

We (Jiménez-Amilburu et al., 2016) and others (Li et al., 2016) have recently reported that CMs in zebrafish and mouse are polarized in the apicobasal axis and that, at least in zebrafish, they undergo apical constriction and depolarization as they delaminate to seed the trabecular layer (Jiménez-Amilburu et al., 2016). However, how apicobasal polarity is regulated in developing CMs remains unknown. In this study, we identified a new role for Crb2a, a member of the Crb complex, during cardiac trabeculation in zebrafish. Crb2a localization in compact layer CMs changes from junctional to apical at the onset of trabeculation. In *crb2a* mutants, we observed novel and severe defects in CM arrangement and morphology, as well as mislocalization of both TJ and AJ proteins. Interestingly, mutant CMs transplanted into wild-type animals were found exclusively in the trabecular layer. These data suggest that the compromised ability of mutant CMs to integrate into the wild-type compact layer makes them more likely to delaminate. Altogether, these data further emphasize the key role of apicobasal polarity in CMs and its tight regulation in the process of cardiac wall maturation.

RESULTS

Crb2a localization changes during cardiac trabeculation in zebrafish

Of the five Crb family genes in zebrafish, *crb2a* is the most highly expressed in the embryonic heart (data not shown). In order to explore the role of Crb2a during cardiac trabeculation, we first used the *Tg(myl7:ras-EGFP)* line (D'Amico et al., 2007) to label CM

Department of Developmental Genetics, Max Planck Institute for Heart and Lung Research, 61231 Bad Nauheim, Germany.

*Author for correspondence (didier.stainier@mpi-bn.mpg.de)

D.Y.R.S., 0000-0002-0382-0026

Received 22 August 2018; Accepted 8 April 2019

Development (2019) 146, dev171207. doi:10.1242/dev.171207

membranes and performed Crb2a immunostaining at several developmental stages (Fig. 1). At 50 hours post fertilization (hpf), before the onset of trabeculation, we observed that Crb2a was highly enriched at apical junctions in compact layer CMs (Fig. 1A-A″). At 74 hpf, once trabeculation has initiated, Crb2a has relocalized to the entire apical membrane of compact layer CMs (Fig. 1B-B″). This switch of Crb2a localization in CMs from junctional to apical was also observed in 3D maximum intensity projection images of hearts at 50 (Fig. 1C,E and Movie 1) and 74 (Fig. 1D,E and Movie 2) hpf. Notably, CMs in the trabecular layer do not appear to express Crb2a (Fig. 1B′,B″). We tested the specificity of the Crb2a antibody by staining *crb2a*$^{-/-}$ hearts and detected no signal (Fig. S1A-B″). Next, to further investigate this junctional to apical relocalization, we performed immunostaining for Crb2a and the TJ marker ZO-1 at 50 and 79 hpf in the *Tg(−0.2myl7:EGFP-podxl)* line (Jiménez-Amilburu et al., 2016), in which the apical side of CMs is labeled by EGFP expression (Fig. S2). At 50 hpf, Crb2a colocalized with ZO-1 at the apical junctions between CMs (Fig. S2A′-A‴), but not with the apical marker podocalyxin. However, at 79 hpf, Crb2a immunostaining labeled the apical side of compact layer CMs, colocalizing with EGFP-Podocalyxin but no longer with the junctional protein ZO-1 (Fig. S2B′,B″). Overall, our results show that Crb2a in compact layer CMs transitions from a prominently junctional to an apical localization at the onset of trabeculation.

Crb2a localization in developing CMs is modulated by blood flow and Nrg2a/Erbb2 signaling

In order to identify regulators of Crb2a localization, we assessed the role of Nrg/Erbb2 signaling and blood flow. As previously reported, blood flow/contractility and Nrg/Erbb2 signaling are essential for cardiac trabeculation (Liu et al., 2010; Peshkovsky et al., 2011; Samsa et al., 2015; Lee et al., 2016; Rasouli and Stainier, 2017). First, to test whether blood flow regulates the localization of Crb2a in CMs, we stopped contractility and blood flow by injecting *tnnt2a*

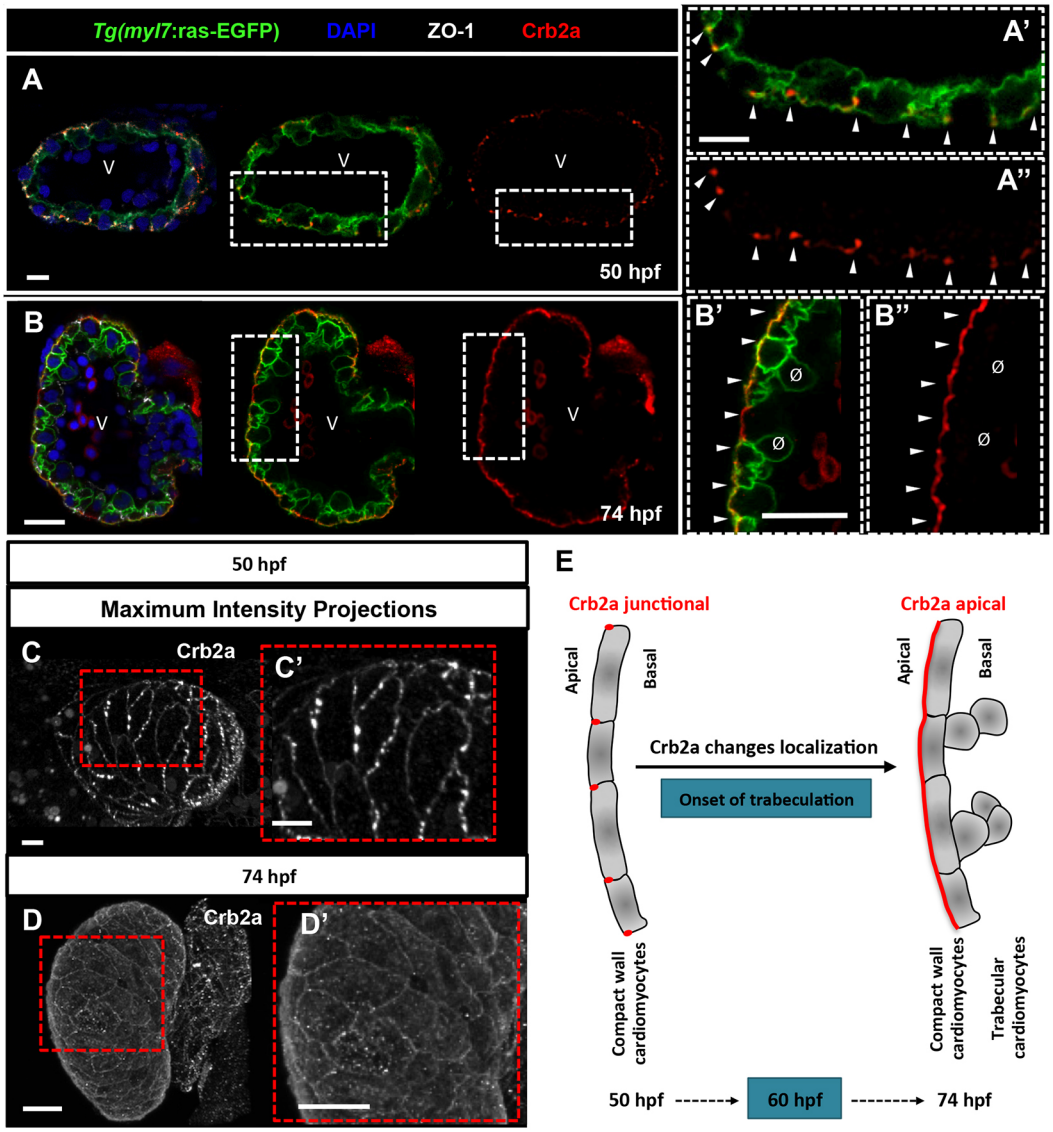

Fig. 1. Crb2a localization changes during cardiac trabeculation in zebrafish. (A-B″) Crb2a immunostaining in *Tg(myl7:ras-EGFP)* hearts at 50 (A-A″, *n*=12) and 74 (B-B″, *n*=15) hpf. At 50 hpf, Crb2a mostly localizes to the apical junctions between CMs (A-A″, arrowheads). At 74 hpf, Crb2a localizes to the entire apical membrane of compact layer CMs (B-B″, arrowheads), and is not observed in delaminated CMs (B′,B″, ø). (C-D′) Maximum intensity projections of ventricles showing junctional Crb2a immunostaining at 50 hpf (C,C′) and apical Crb2a immunostaining at 74 hpf (D,D′). (E) Schematic illustration of Crb2a relocalization in CMs from junctional to apical during the onset of trabeculation. V, ventricle. Scale bars: 20 µm.

Development (2019) 146, dev171207. doi:10.1242/dev.171207

morpholinos (MOs) (Sehnert et al., 2002) into one-cell stage embryos. Uninjected larvae at 80 hpf displayed apical localization of Crb2a in compact layer CMs (Fig. 2A-A″), while *tnnt2a* morphants retained Crb2a localization at the junctions between compact layer CMs (Fig. 2B-B″). Next, we treated *Tg(myl7:ras-EGFP)* embryos at 54 hpf, i.e. before trabeculation starts, with 10 µM PD168393, an Erbb2 inhibitor, or with DMSO as a control. At 96 hpf, Crb2a immunostaining was observed along the entire apical membrane of compact layer CMs in DMSO-treated larvae (Fig. 2C-C″,E), while Erbb2 inhibitor-treated larvae displayed a significant increase in junctional Crb2a (average of 14.69 junctions between CMs with Crb2a enrichment, compared with 4.57 in DMSO-treated larvae) (Fig. 2D-D″,E). To test whether activation of Nrg/Erbb2 signaling caused the opposite phenotype, we overexpressed the Erbb2 ligand Nrg2a in CMs. CMs expressing the *myl7:nrg2a-p2a-tdTomato* transgene displayed increased apical localization of Crb2a at 52 hpf, a stage when Crb2a is junctionally located in control hearts (Fig. 2F-F″). Altogether, these data indicate that blood flow and Nrg2a/Erbb2 signaling regulate Crb2a localization in CMs.

crb2a$^{-/-}$ hearts display disrupted compact wall integrity and fail to form trabeculae

To investigate the role of Crb2a during cardiac trabeculation, we studied the *ome*/*crb2a* mutant (Malicki et al., 1996; Omori and Malicki, 2006). First, to characterize CM morphology during trabeculation, we crossed the *crb2a*$^{-/-}$ with the CM membrane reporter line *Tg(myl7:MKATE-CAAX)* (Lin et al., 2012). At 80 hpf, after the onset of cardiac trabeculation, *crb2a*$^{-/-}$ larvae exhibit a more rounded and smaller ventricle compared with *crb2a*$^{+/+}$ siblings (Fig. 3A,B). At this stage, we observed that while *crb2a*$^{+/+}$ ventricle present a single layer of CMs in the compact wall with a few delaminated CMs (Fig. 3A′-A″,F,G), the *crb2a*$^{-/-}$ cardiac wall was composed of two or three layers of CMs and appeared disorganized (Fig. 3B′-B‴,F′,G). Morphologically, CMs in the mutant ventricles appeared more elongated than those in wild-type siblings (Fig. 3A′,A″,B′,B″). To further investigate this phenotype, we measured the circularity of compact layer CMs in the outer curvature at 80 hpf, and observed a significant difference (Fig. 3E). Mutant larvae at 98 hpf did not exhibit myocardial protrusions into the ventricular lumen and failed to form trabeculae

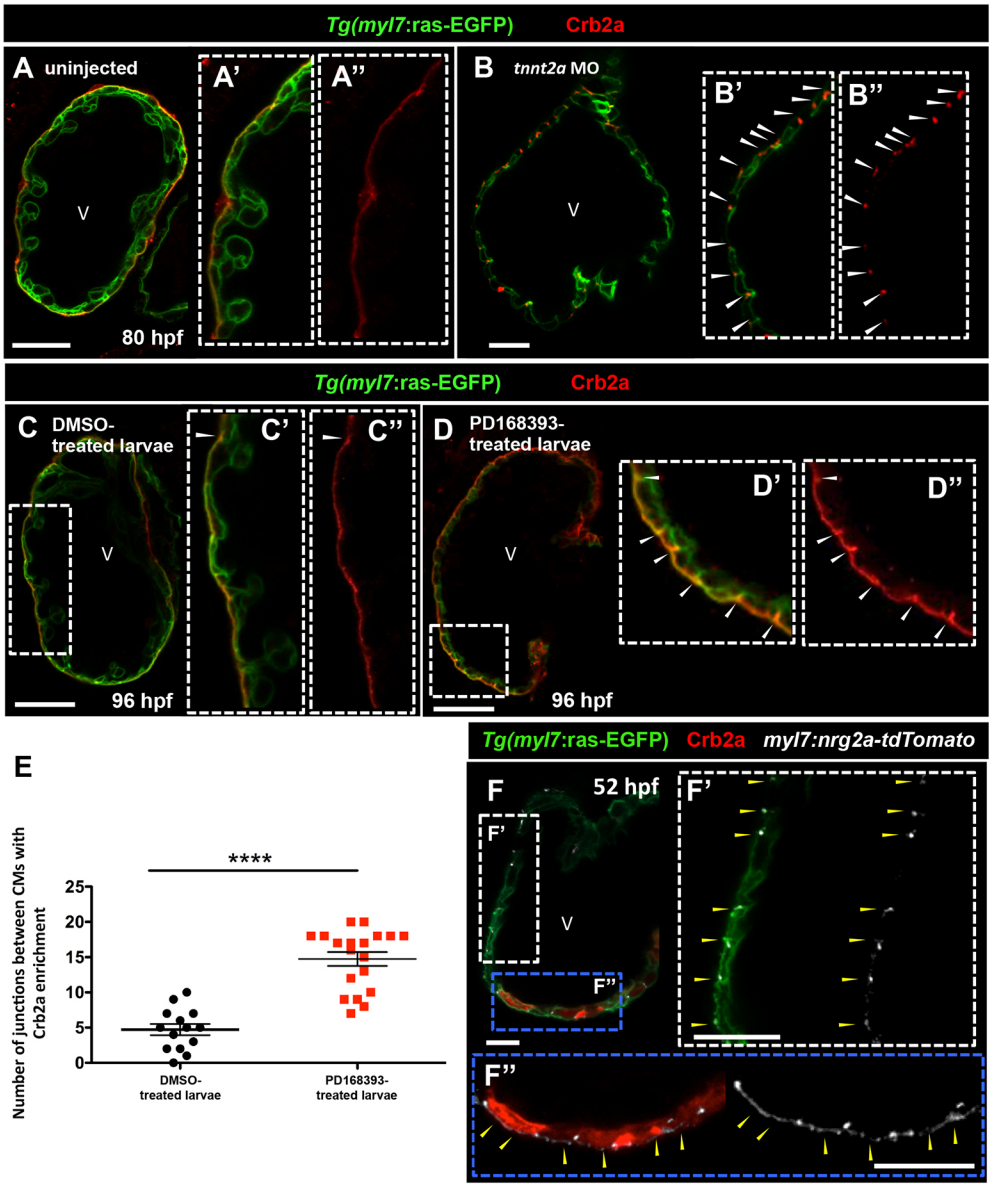

Fig. 2. Crb2a localization in developing CMs is modulated by blood flow and Nrg2a/ErbB2 signaling. (A-B″) Crb2a immunostaining in *Tg(myl7:ras-EGFP)* control (A, *n*=8) and *tnnt2a* morphant (B, *n*=8) hearts at 80 hpf. Higher-magnification images show apical localization of Crb2a in control (A′,A″) and *tnnt2a* morphant hearts (B′,B″); arrowheads indicate junctional localization of Crb2a between CMs. (C-D″) Crb2a immunostaining in 96 hpf *Tg(myl7:ras-EGFP)* hearts treated between 54 and 96 hpf with DMSO (C-C″, *n*=14) or PD168393 (D-D″, *n*=19); arrowheads indicate Crb2a enrichment at the junctions between CMs. (E) Number of junctions between CMs with Crb2a enrichment. Each dot or square represents data from one heart. Data are mean±s.e.m. ****P<0.0001 by Student's *t*-test. (F) Crb2a immunostaining in 52 hpf *Tg(myl7:ras-EGFP)* embryos injected at the one-cell stage with a myocardial-specific *nrg2a* construct (*myl7:nrg2a-p2a-tdTomato*) (*n*=8). (F′,F″) Higher-magnification images show junctional localization of Crb2a in non-*nrg2a*-expressing CMs (arrowheads in white dashed box, F′) and apical Crb2a localization in *nrg2a*-expressing CMs (arrowheads in blue dashed box, F″). V, ventricle. Scale bars: 20 µm.

Development (2019) 146, dev171207. doi:10.1242/dev.171207

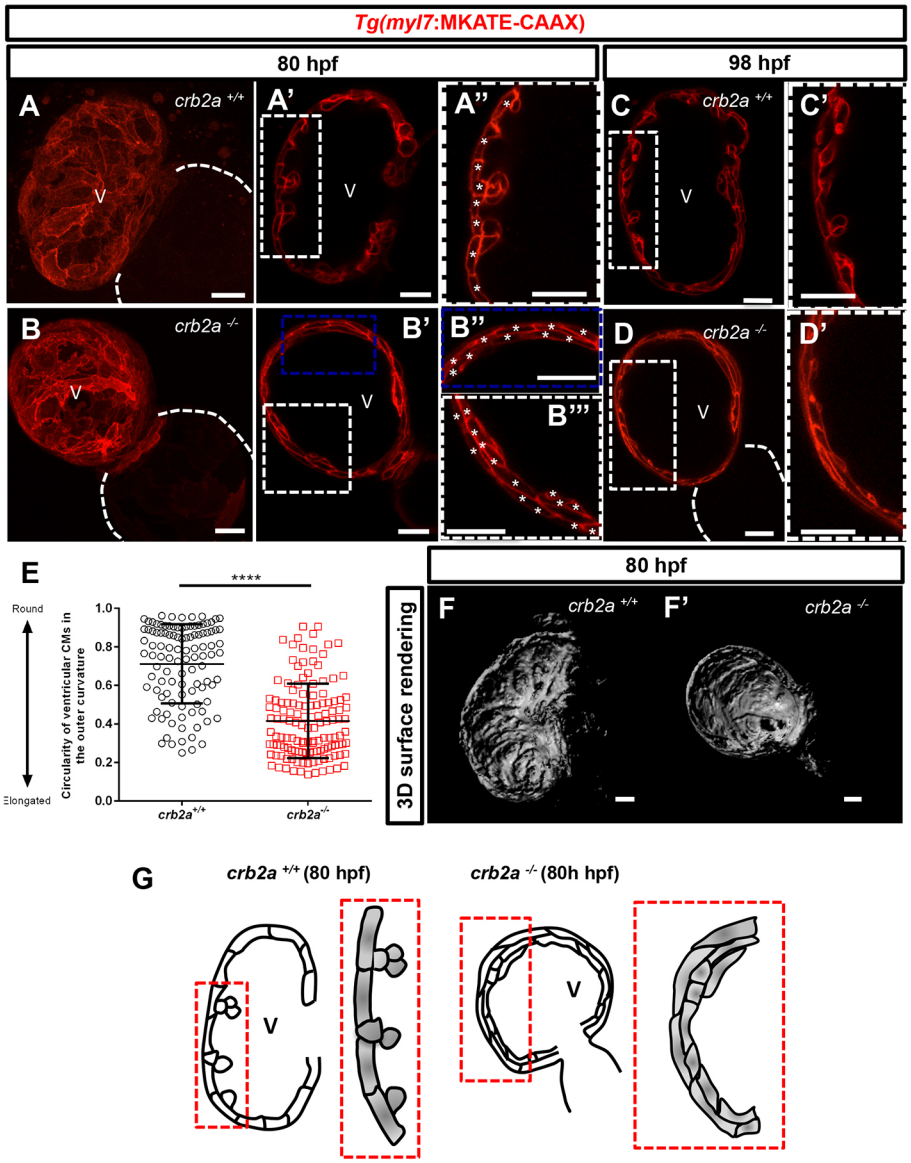

Fig. 3. *crb2a*$^{-/-}$ hearts display disrupted compact wall integrity and fail to form trabeculae. (A-B″) Confocal images (maximum intensity projections) of 80 hpf *Tg(myl7:MKATE-CAAX) crb2a*$^{+/+}$ (A-A″) and *crb2a*$^{-/-}$ (B-B″) hearts. (A-D′) Confocal images (mid-sagittal sections) of *Tg(myl7:MKATE-CAAX)* hearts of *crb2a*$^{+/+}$ (A-A″, *n*=8; C,C′, *n*=8) and *crb2a*$^{-/-}$ (B-B″, *n*=14; D,D′, *n*=14) larvae at 80 and 98 hpf. Asterisks in A″,B″ and B‴ indicate individual CMs in the compact wall. (E) Circularity of ventricular CMs (outer curvature) in 80 hpf *crb2a*$^{+/+}$ (*n*=7 hearts) and *crb2a*$^{-/-}$ (*n*=10 hearts) larvae. Each point represents data from an individual CM. Data are mean±s.e.m. ****P<0.0001 by Student's *t*-test. (F,F′) 3D surface rendering images of 80 hpf *crb2a*$^{+/+}$ (F) and *crb2a*$^{-/-}$ (F′) ventricles. (G) Schematic illustration of the myocardial wall in 80 hpf *crb2a*$^{+/+}$ and *crb2a*$^{-/-}$ ventricles. V, ventricle. Scale bars: 20 µm.

(Fig. 3D,D′), while wild-type siblings at this stage presented a complex trabecular network (Fig. 3C,C′). To examine whether the multilayering phenotype was present before the onset of trabeculation, we imaged 52 hpf embryos, and found that, although *crb2a*$^{+/+}$ ventricles consist of a single layer of CMs at this stage (Fig. S3A,A′,D), 19 of 22 mutant ventricles examined displayed multilayering (Fig. S3B,B′,D) and the other three exhibited a single layer of CMs (Fig. S4C,C′,D). We also tested whether defects in cardiac jelly degradation might account for this phenotype by imaging *crb2a*$^{-/-}$ in the *Tg(kdrl:EGFP)* (Jin et al., 2005); *Tg(myl7:MKATE-CAAX)* background to label, respectively, endocardial and myocardial cells. We did not observe obvious differences in cardiac jelly thickness between *crb2a*$^{+/+}$ (Fig. S4A-C′,E) and *crb2a*$^{-/-}$ (Fig. S4B-D′,E) siblings at 80 or 100 hpf.

Next, we studied the early stages of cardiac development in *crb2a*$^{-/-}$ animals. At 36 hpf, *crb2a*$^{+/+}$ and *crb2a*$^{+/-}$ hearts have looped (Fig. S5A,B), whereas *crb2a*$^{-/-}$ hearts remained in the midline or exhibited delayed looping (Fig. S5C,C′). We also analyzed circulation at 48 hpf, and found that 40% of the mutants exhibited few or no circulating blood cells, while the other 60% exhibited wild-type-like circulation (Fig. S6D). To evaluate cardiac performance in *crb2a*$^{-/-}$ hearts, we measured atrial fractional shortening (FS) (Fig. S6A-C′). Bright-field images of the beating heart were acquired at 48 hpf and FS was calculated in *crb2a*$^{+/+}$ and *crb2a*$^{+/-}$ animals, as well as in *crb2a* homozygous mutants with and without circulation (Movies 3-6). This analysis showed that *crb2a*$^{-/-}$ animals without circulation exhibit a significant decrease in atrial FS compared with *crb2a*$^{+/+}$ or *crb2a*$^{+/-}$, while mutants with circulation exhibit a slight, but not significant, reduction in atrial FS (Fig. S6E). In order to test whether this reduction in cardiac function was due to sarcomere defects, we performed α-actinin immunostaining in *Tg(myl7:MKATE-CAAX); crb2a*$^{-/-}$ hearts at 80 hpf, and observed no obvious differences in sarcomeric structure between *crb2a*$^{+/+}$ and *crb2a*$^{-/-}$ animals (Fig. S6F-G′). To avoid any confounding effects, all subsequent experiments in this manuscript were performed exclusively with *crb2a*$^{-/-}$ animals exhibiting wild-type-like circulation. Taken together, these data show that Crb2a plays an important role during cardiac trabeculation.

Development (2019) 146, dev171207. doi:10.1242/dev.171207

Most inner layer CMs in *crb2a*$^{-/-}$ remain polarized in the apicobasal axis

To gain further insight into CM polarization in *crb2a*$^{-/-}$ animals, we crossed the mutation into the *Tg(−0.2myl7:EGFP-podxl)* line. As previously reported (Jiménez-Amilburu et al., 2016), EGFP-Podocalyxin localizes to the apical side of compact layer CMs and covers the entire cortex of delaminated CMs in wild-type ventricles at 80 hpf (Fig. 4A-A′,C). In *crb2a*$^{-/-}$ ventricles, CMs forming the inner layer of the wall were also polarized, as per their apical localization of EGFP-Podocalyxin (Fig. 4B,B′,C). These observations were confirmed by assessing EGFP-Podocalyxin colocalization with *Tg(myl7:MKATE-CAAX)* expression and quantifying the number of depolarized CMs in *crb2a*$^{+/+}$ and *crb2a*$^{-/-}$ ventricles (Fig. 4C). In order to test whether the multilayering phenotype of *crb2a*$^{-/-}$ CMs was due to an increase in CM number, we assessed cell proliferation in mutant hearts. To quantify proliferating CMs, we imaged embryos expressing the CM nuclear transgene *Tg(myl7:nlsDsRED)* (Rottbauer et al., 2002), as well as the *Tg(myl7:VenusGeminin)* line (Jiménez-Amilburu et al., 2016), which marks actively proliferating CMs, and examined maximum intensity projection images at 80 hpf (Fig. S7A-C). We found that the number of total CMs and proliferating CMs was similar in *crb2a*$^{+/+}$, *crb2a*$^{+/-}$ and *crb2a*$^{-/-}$ animals (Fig. S7D,E). Taken together, these data show that Crb2a plays a role in modulating CM polarity and specifically prevent CM delamination from the compact layer in the absence of Nrg2a/ErbB2 signaling.

Tight and adherens junction proteins are mislocalized in *crb2a*$^{-/-}$ hearts

The Crb complex regulates the localization of TJ and AJ proteins during cellular rearrangements in fly epithelia (Grawe et al., 1996; Izaddoost et al., 2002). To assess whether this regulation also takes place during cardiac development, we immunostained the AJ reporter line *TgBAC(cdh2:Cdh2-EGFP)* (Revenu et al., 2014) for Crb2a and ZO-1. At 54 hpf, before the onset of trabeculation, Crb2a colocalizes with ZO-1 at CM junctions (Fig. S8A-A″″,C). At this stage, N-Cadherin localizes laterally in CMs showing no overlap with Crb2a or ZO-1 (Fig. S8A-A″″,C). Once trabeculation initiates and Crb2a becomes apically localized in compact layer CMs, ZO-1 remains junctional and N-Cadherin extends basolaterally (Fig. S8B-B″″,C). Next, we analyzed whether TJ and AJ protein localization was affected in *crb2a*$^{-/-}$ ventricles. First, we performed immunostaining for ZO-1 in *Tg(myl7:MKATE-CAAX); crb2a*$^{-/-}$ at 79 hpf. Maximum intensity projections and single-plane images of *crb2a*$^{+/+}$ larvae show junctional localization of ZO-1 between compact layer CMs (Fig. S9A-B′). However, at the same stage, ZO-1 was mislocalized in both compact and inner layer *crb2a*$^{-/-}$ CMs (Fig. 5A-A″″,B-B″″). In order to be able to study *in vivo* CM TJ protein dynamics more closely, we generated a *Tg(-0.2myl7:ZO-1-EGFP)* line. Using this line, we were able to reproduce the endogenous localization of ZO-1 during cardiac trabeculation in both mutant and wild-type siblings (Fig. S10). We also performed immunostaining for N-Cadherin in *Tg(myl7:MKATE-CAAX)*; *crb2a*$^{-/-}$ larvae at 79 hpf. Analysis of maximum intensity projection images showed that the lateral

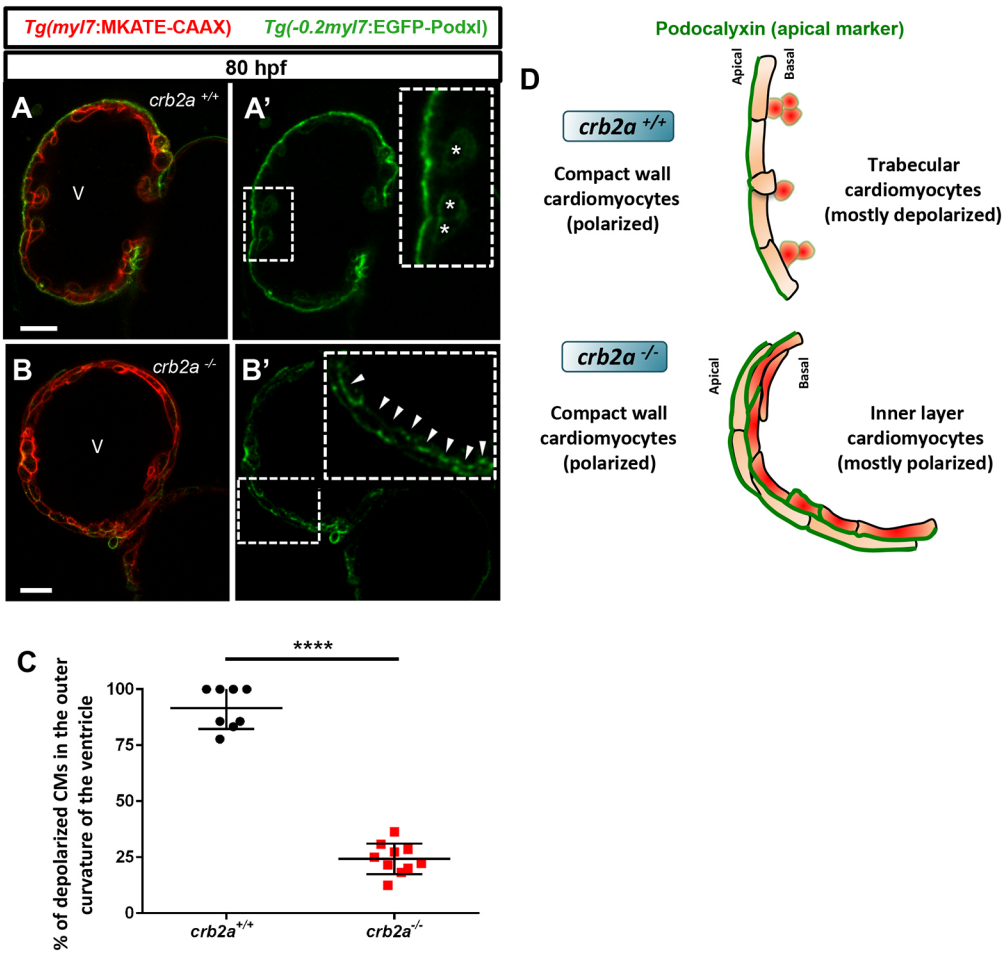

Fig. 4. Most inner layer CMs in *crb2a*$^{-/-}$ remain polarized in the apicobasal axis. (A-B′) Confocal images (mid-sagittal sections) of 80 hpf *Tg(−0.2myl7:EGFP-podxl); Tg(myl7:MKATE-CAAX); crb2a*$^{+/+}$ (A) and *crb2a*$^{-/-}$ (B) hearts. Asterisks in A′ mark delaminated CMs and arrowheads in B′ indicate polarized CMs. (C) Percentage of depolarized CMs in the outer curvature of the ventricle of 80 hpf *crb2a*$^{+/+}$ (n=8) and *crb2a*$^{-/-}$ (n=10) larvae. Data are mean±s.e.m. ****P<0.0001 by Student's t-test. (D) Schematic illustration of A′ and B′ showing depolarized CMs in the trabecular layer of *crb2a*$^{+/+}$ hearts and polarized CMs in the inner layers of *crb2a*$^{-/-}$ hearts. V, ventricle. Scale bars: 20 µm.

Development (2019) 146, dev171207. doi:10.1242/dev.171207

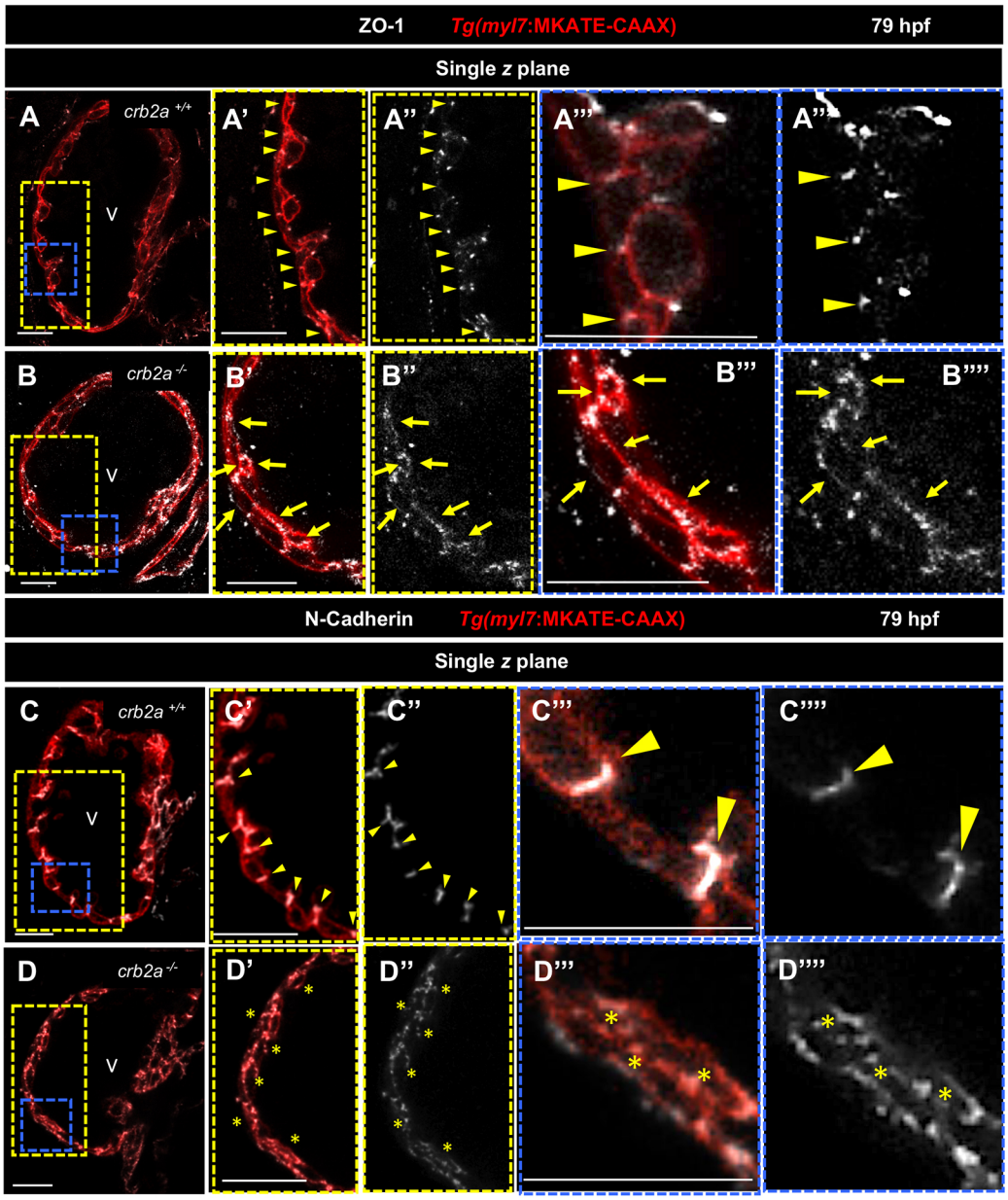

Fig. 5. Tight and adherens junction proteins are mislocalized in *crb2a*$^{-/-}$ hearts. (A-B″″) Confocal images (mid-sagittal sections) of 79 hpf *Tg(myl7:MKATE-CAAX); crb2a*$^{+/+}$ (A-A″″) and *crb2a*$^{-/-}$ (B-B″″) hearts immunostained for ZO-1. Single-plane images show that ZO-1 localizes to the junctions between CMs in *crb2a*$^{+/+}$ (A-A″, arrowheads, *n*=10), but that this junctional pattern is fragmented in *crb2a*$^{-/-}$ (B-B″, arrows, *n*=16). High magnifications of single-plane images show the junctional localization of ZO-1 between CMs in *crb2a*$^{+/+}$ (A‴,A⁗, arrowheads), while in *crb2a*$^{-/-}$, ZO-1 immunostaining appears punctate in both apical and basal CM membranes (B‴,B⁗, arrows). (C-D″″) Confocal images (mid-sagittal sections) of 79 hpf *Tg(myl7:MKATE-CAAX); crb2a*$^{+/+}$ (C-C″″) and *crb2a*$^{-/-}$ (D-D″″) hearts immunostained for N-Cadherin. Single-plane images show that N-Cadherin localizes to the junctions between CMs in *crb2a*$^{+/+}$ (C-C″, arrowheads, *n*=7) but is mislocalized in *crb2a*$^{-/-}$ (D-D″, asterisks, *n*=15). High magnifications of single-plane images show the lateral localization of N-Cadherin between CMs in *crb2a*$^{+/+}$ (C‴,C⁗, arrowheads), while in *crb2a*$^{-/-}$, N-cadherin localization appears more punctate in both the apical and basal membranes of compact layer CMs (D‴,D⁗, asterisks). V, ventricle. Scale bars: 20 µm.

localization of N-Cadherin between compact layer CMs was lost in mutant hearts (Fig. S9C-D′), appearing punctate in both apical and basal membranes (Fig. 5C-C″″,D,D″″). These data indicate that junctional reorganization in CMs is likely to play a role during CM delamination, and suggest a role for Crb2a in regulating TJ and AJ protein localization in developing CMs.

Crb2a regulates CM behavior cell-autonomously

To gain further insight into Crb2a function during cardiac trabeculation, we generated chimeric embryos by transplanting at the mid-blastula stage *Tg(myl7:MKATE-CAAX); crb2a*$^{+/+}$, *crb2a*$^{+/-}$ or *crb2a*$^{-/-}$ cells into *Tg(myl7:ras-EGFP); crb2a*$^{+/+}$ animals. After transplantation, larvae were imaged at 100 hpf and donors were subsequently genotyped. We found that *crb2a*$^{+/+}$ and *crb2a*$^{+/-}$ CMs in *crb2a*$^{+/+}$ ventricles localized in both the compact and trabecular layers. Strikingly, *crb2a*$^{-/-}$ CMs in *crb2a*$^{+/+}$ ventricles were found exclusively in the trabecular layer (Fig. 6A-C). To extend these observations, we quantified the number of donor-derived CMs in the compact and trabecular layers in chimeric larvae at 100 hpf, and found that 100% of the *crb2a*$^{-/-}$ CMs populated the

Development (2019) 146, dev171207. doi:10.1242/dev.171207

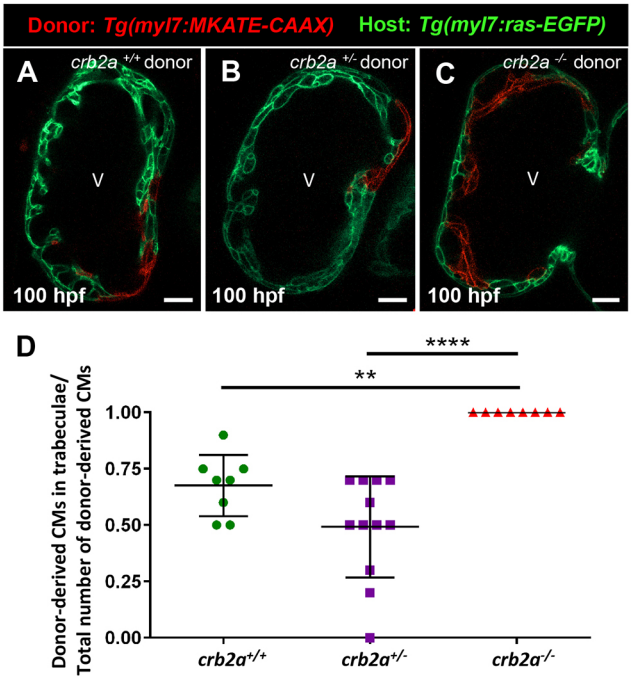

Fig. 6. Crb2a regulates CM behavior cell-autonomously. (A-C) Confocal images (mid-sagittal sections) of mosaic 100 hpf *crb2a*$^{+/+}$ *Tg(myl7:ras-EGFP)* host hearts transplanted with *Tg(myl7:MKATE-CAAX); crb2a*$^{+/+}$, *crb2a*$^{+/-}$ or *crb2a*$^{-/-}$ cells. (D) Percentage of donor-derived CMs in trabeculae versus total number of donor-derived CMs. Each point represents data from one heart. One-way analysis of variance (ANOVA) was performed corrected by Tukey's multiple comparisons test. $^{**}P<0.01$; $^{****}P<0.0001$. V, ventricle. Scale bars: 20 µm.

trabecular layer of *crb2a*$^{+/+}$ ventricles (Fig. 6D). These data show that CMs leave the compact layer in the absence of Crb2a function, indicating that Crb2a functions cell-autonomously in CMs to regulate this behavior.

DISCUSSION

Cardiac trabeculation in zebrafish has been proposed as an EMT-like process whereby a subset of CMs undergo apical constriction and lose apicobasal polarity as they delaminate to seed the trabecular layer (Liu et al., 2010; Staudt et al., 2014; Cherian et al., 2016; Jiménez-Amilburu et al., 2016). However, it remains unclear how CM apicobasal polarity is regulated. Here, we set out to investigate whether and how Crb2a, a member of the Crb polarity complex, regulates cardiac trabeculation. In this study, we present *in vivo* evidence that Crb2a has a key role in maintaining CM apicobasal polarity, as well as in regulating junctional rearrangements during early cardiac development.

The coordinated action of different proteins that modulate apicobasal identity, together with cytoskeletal and junctional rearrangements, maintains cell shape and tissue integrity (Hurd et al., 2003; Kempkens et al., 2006). For example, Crb has a conserved role in a number of epithelial tissues, regulating apicobasal polarity and maintaining junctional integrity during morphogenetic processes (Grawe et al., 1996; Izaddoost et al., 2002). Here, we found that the Crb polarity protein Crb2a shifts its localization in CMs from junctional to apical just prior to the onset of trabeculation. Accordingly, CMs have been reported to exhibit substantial cellular plasticity during trabeculation, losing their cobblestone-like shape once they start delaminating (Liu et al., 2010; Staudt et al., 2014). Our observations are consistent with previous reports in *Drosophila* where during follicular morphogenesis as cells change shape, Crb is lost from the marginal zone (the most apical surface), relocalizes to the AJ and subsequently reappears at the marginal zone (Sherrard and Fehon, 2015; Wu et al., 2016). We found that blocking Nrg/ErbB2 signaling leads to relocalization of Crb2a from the junctions to the apical surface of CMs. Interestingly, in *Drosophila*, depletion of cytoskeletal proteins required for Crb localization leads to relocalization of apical Crb to the junctions (Sherrard and Fehon, 2015). These data indicate that Crb2a localization is very dynamic and that Nrg/ErbB2 signaling, which is essential for cardiac trabeculation, is required for its junctional to apical shift.

Mutations in *CRB2* in humans and *Crb2* in mouse cause cardiac malformations (Xiao et al., 2011; Slavotinek et al., 2015; Jaron et al., 2016). Similarly, we found that zebrafish lacking Crb2a display a compact ventricular wall composed of multiple disorganized layers of CMs. This phenotype is reminiscent of that observed during *Drosophila* oogenesis, where early loss of Crb leads to multilayering (Tanentzapf et al., 2000; Pénalva and Mirouse, 2012). While delaminating CMs in wild-type ventricles lose their apicobasal identity (Jiménez-Amilburu et al., 2016), most CMs in *crb2a* mutants remain polarized, including those in the inner layers. These data suggest that inner layer CMs in *crb2a* mutants are not trabecular CMs.

During epithelial morphogenesis, changes in cell shape and the localization of junctions require the tight regulation of junctional proteins and the cytoskeleton (Costa et al., 1998; Raich et al., 1999; Martin et al., 2010). We observed that *crb2a* mutant CMs display mislocalization of TJ and AJ proteins. Similarly, loss of Crb in epithelial cells in *Drosophila* causes defects in cell-cell adhesion and tissue integrity (Tepass and Knüst, 1990; Grawe et al., 1996; van de Pavert et al., 2004; Letizia et al., 2013; Flores-Benitez and Knüst, 2015). Certainly, the polarity complex protein Crumbs regulates not only the stability but also the localization of junctions in *Drosophila* salivary glands (Xu et al., 2008) and *Drosophila* eyes (Fan et al., 2003). Therefore, we hypothesize that the lack of Crb2a in zebrafish mutant hearts leads to mislocalization of CM junction proteins, thereby affecting compact layer architecture and in turn CM delamination/migration. Moreover, during tissue morphogenesis, mechanical tension plays a key role in controlling actomyosin networks and cell-cell junction remodeling to maintain cell shape (Lecuit et al., 2011; Lecuit and Yap, 2015). Compact layer CMs are subjected to mechanical forces necessary for ventricular chamber maturation (Cherian et al., 2016). In view of these data, we propose that loss of cell-cell adhesions in *crb2a* mutant hearts is at least partially responsible for the CM multilayering phenotype coming from the collapse of the CM monolayer prior to the onset of delamination. Indeed, multilayering can be observed in *crb2a* mutants at early stages of development. As a consequence, ventricular shape is significantly affected in *crb2a*$^{-/-}$, and CMs remaining in the compact layer flatten out. However, how the actin cytoskeleton is affected in *crb2a*$^{-/-}$ CMs remains to be investigated.

In mosaic embryos, we observed that all *crb2a* mutant CMs in wild-type ventricles become part of the trabecular layer. Similarly, *wwtr1* mutant CMs in wild-type ventricles exhibit a preference to enter this layer (Lai et al., 2018). The cardiac phenotypes of *wwtr1* and *crb2a* mutants are similar in the sense that they both exhibit CM multilayering, although it is more pronounced and is observed at an earlier stage in *crb2a* mutants. Interestingly, we found that Crb2a immunostaining was hardly detectable in *wwtr1* mutant hearts (Fig. S11), suggesting that a reduction in Crb2a expression leads to the mislocalization of AJ proteins in *wwtr1* mutant hearts (Lai et al.,

Development (2019) 146, dev171207. doi:10.1242/dev.171207

2018). In summary, the lack of Crb2a in zebrafish CMs affects their ability to remain in a monolayer, subsequently leading to the lack of trabeculae.

MATERIALS AND METHODS

Ethics statement

All experiments using zebrafish were performed in accordance with German animal protection laws and approved by the local governmental animal protection committee. Zebrafish were maintained according to standard protocols (wiki.zfin.org/display/prot/General+Methods+for+Zebrafish+Care).

Transgenic and mutant zebrafish lines

Transgenic lines used in this study are as follows: *Tg(−0.2myl7:EGFP-podocalyxin)*^{bns103} (Jiménez-Amilburu et al., 2016), abbreviated *Tg(−0.2myl7:EGFP-podxl)*; *Tg(myl7-MKATE-CAAX)*^{sd11} (Lin et al., 2012), abbreviated *Tg(myl7:MKATE-CAAX)*; *Tg(myl7:EGFP-Has.HRAS)*^{s883} (D'Amico et al., 2007), abbreviated *Tg(myl7:ras-EGFP); Tg(myl7:mVenus-gmnn)*^{ncv43Tg} (Jiménez-Amilburu et al., 2016), abbreviated *Tg(myl7:mVenus-gmnn); Tg(kdrl:EGFP)*^{s843} (Jin et al., 2005), abbreviated *Tg(kdrl:EGFP); TgBAC(cdh2:Cdh2-EGFP,crybb1:ECFP)*^{zf517} (Revenu et al., 2014), abbreviated *TgBAC(cdh2:Cdh2-ECFP); Tg(-5.1myl7:DsRed2-NLS)*^{f2Tg} (Rottbauer et al., 2002) and abbreviated *Tg(myl7:nlsDsRed)*.

The mutant allele used in this study is *crb2a*^{m598} (Omori and Malicki, 2006). To screen for adult carriers or discriminate between wild-type, *crb2a*$^{+/−}$ and *crb2a*$^{−/−}$ at embryonic/larval stages, we used genomic DNA extracted from clipped fins. PCR1 was performed using the following primers: 5′-TCAGGCTTGTCCTTCAAGTC-3′ and 3′-TTACTTGGCTCAGGTG-TGTC-5′. The product from PCR1 was then used to perform PCR2 using the following primers: 5′-TGTAAAACGACGGCCAGTTCAAGCATGCAGA GTTGAAG-3′ and 3′-AGGAAACAGCTATGACCATTATGCAAGACA-CTGGCACTC-5′. The product from PCR2 was sent for sequencing with an M13 universal primer (5′-TTACTTGGCTCAGGTGTGTC-3′). Chromatograms were used to distinguish between wild type (TGACTGT-TAC**A**GACCCC), *crb2a*$^{+/−}$ (TGACTGTTAC**A/T**GACCCC) and *crb2a*$^{−/−}$ (TGACTGTTAC**T**GACCCC) (differing nucleotides are indicated in bold).

Generation of transgenic zebrafish line

The *pTol2−0.2myl:EGFP-ZO-1* plasmid was generated using the Cold Fusion Cloning Kit (System Biosciences, MC101A-SBI). EGFP-ZO-1 was amplified using the Phusion Tag HF Polymerase and the following primers: forward, 5′-CAAAGCAGACAGTGAGCTAGCATGGTGAGCAAGGG-CGAGGA-3′; and reverse, 5′-TCCCCCGGGCTGCAGGAATTCCTAG-AGGCTCGAGATGGGAA-3′. The PCR product was subsequently cloned into a Tol2 enabled vector with the −0.2 kb *myl7* promoter. After Cold Fusion Cloning, colonies containing the construct were sent for sequencing for validation.

Chemical treatments

Embryos were treated with 10 µM of the ErbB2 inhibitor PD168393 at 54 hpf. For all treatments, ten embryos per well were placed in 1 ml PTU egg water in 12-well plates containing the corresponding drug. DMSO was used as a control. In the case of PD168393, drugs were added into egg water containing PTU and 1% DMSO to help with solubilization.

myl7-nrg2a-p2a-tdTomato construct injection

For mosaic expression of *nrg2a* in CMs, 15 pg of *myl7-nrg2a-p2a-tdTomato* plasmid DNA was injected together with 10 pg of Tol2 mRNA at the one-cell stage into the cell.

Whole-mount immunostaining of zebrafish embryos/larvae

Embryos were treated with PTU to avoid pigmentation and dechorionated using pronase at 1 dpf. Embryos/larvae were fixed at the stage of interest in 2 ml Fish fix buffer [1×PBS, 120 µl 1 M $CaCl_2$, 40 g sucrose with PFA (pH 7.35)] overnight at 4°C on a nutator. The next day, the Fish fix buffer was removed and embryos were washed three times for 15 min with PBS/0.1% Tween20 followed by manual removal of the yolk of the embryos/larvae manually using forceps. Deyolking was followed by permeabilization with proteinase K (3 µm/ml) in 1 ml PBS/0.1%Tween20 (50-54 hpf for 20 min; 72 hpf for 50 min; 79-80 hpf for 1 h). After permeabilization embryos/larvae were rinsed quickly with PBDT to stop the proteinase K reaction. Then, embryos/larvae were washed three times for 15 min in PBDT. Blocking was carried out using blocking buffer [PBS/0.1% Tween + 10% sheep serum + 4% (20% Triton-X) + 5% (20% BSA)] for 2-3 h. Embryos/larvae were then incubated with the corresponding primary antibodies with incubation buffer overnight at 4°C in the rotator (shaking gently). The following primary antibodies with their corresponding concentrations were used: Crb2a, 1:500 (Zou et al., 2012) was used in Figs 1 and 2; Crb2a, 1:50 (ZIRC, zs-4) was used in the rest of the figures; ZO1, 1:2000 (Invitrogen, 33-9100); EGFP, 1:500 (Aves Lab, gfp-1020); α-actinin, 1:1000 (Sigma, A7811); N-Cadherin, 1:250 (Abcam, ab12221); and tRFP, 1:500 (Evrogen, AB233). The next day, following incubation, the primary antibodies were removed and embryos/larvae were washed four times for 20 min with PBDT. Embryos/larvae were incubated with the secondary antibodies in incubation buffer: PBS/0.1% Tween + 1% sheep serum + 4% (20%Triton-X) + 5% (20% BSA) for 4 h at room temperature in the rotator (shaking gently). All secondary antibodies [Alexa Fluor 488 anti-chicken (A11039), Alexa Fluor 488 anti-rabbit (A11034), Alexa Fluor 488 anti-mouse (A11029), Alexa Fluor 568 anti mouse (A11004) and Alexa Fluor 647 anti-mouse (A21236)] were obtained from Life Technologies and used at 1:500. Next, secondary antibodies were removed and embryos/larvae were washed first with DAPI in PBS/Tween20 for 10 min, followed by 6×15 min washes in PBS/Tween20. All these steps were performed in the dark. DAPI (Life Technologies) was used at 1:10,000. Once the washes were finished, embryos/larvae were kept in PBS/0.1%Tween20 at 4°C in the dark until the day of imaging.

Imaging 36 hpf hearts: embryo preparation

Embryos were treated with PTU to avoid pigmentation and dechorionated using pronase at 1 dpf. At 36 hpf, embryos were fixed with 4% PFA overnight at 4°C. PFA was removed the next day and embryos were washed with PBS/0.1%Tween20 twice for 10 min. After PFA removal, the heads of the embryos were cut using forceps and a blade. The cut was performed right under the head in an angle of 15° with respect to the base of the head. Removing the head at early stages helps to visualize the heart. Embryos were kept in PBS/0.1%Tween20 at 4°C until the day of imaging.

Cell transplantation

Donor cells for transplantation were obtained from embryos from *Tg(myl7:MKATE-CAAX) crb2a*$^{+/−}$ incrosses. Wild-type host embryos were obtained from crossing *Tg(myl7:ras-EGFP)* animals. For transplantation, embryos were first dechorionated by treating with 1 mg/ml pronase in Danieau buffer and then maintained on agarose-coated petri dishes until blastomere stages. Embryos were then transferred into 12-well plates where each well was filled with agarose. Donor embryos were kept in Ringer's buffer containing penicillin/streptomycin, and donor cells were transplanted into two or three different wild-type host embryos along the blastoderm margin at mid-blastula stages. Donor larvae were maintained alive for genotyping. Prior to imaging, selection of mosaic larvae was carried out by screening for those expressing both the MKATE-CAAX and ras-EGFP transgenes. Imaging was carried out using an LSM800 confocal microscope (Zeiss) and the contribution of the donor-derived cells to the trabecular or compact layer was quantified by analyzing the whole ventricle plane by plane using the ZEN software (Zeiss).

Quantification of trabecular versus compact layer CMs in transplanted hearts

Confocal images were processed and analyzed using the ZEN Black Software (Zeiss). Quantification was started at the ventricular mid-sagittal plane and counted 12 planes up and 12 planes down at an increment of 1 µm per plane, and this set of 24 planes was used for analysis. The number of compact layer and trabecular CMs was counted in this set of 24 planes. The percentage of trabecular CMs was calculated by dividing the number of trabecular CMs by the total number of CMs.

Fractional shortening (FS) measurement

Bright-field images of wild-type, *crb2a*$^{+/-}$ and *crb2a*$^{-/-}$ beating hearts were acquired at 48 hpf using a spinning disc confocal microscope. Zebrafish embryos were mounted in low melting agarose containing 0.01% (w/v) tricaine in a glass-bottomed dish. *Z*-stacks of beating hearts were imaged at 50 frames/s. The width of the atrium at the maximum systolic and diastolic phases was measured in three different non-consecutives frames and the FS was calculated as (diastole length−sistole length/diastole length)×100.

Measurement of cardiac jelly thickness

Four different measurements of cardiac jelly thickness were taken at the mid-sagittal ventricular plane of 80 and 100 hpf hearts. The ZEN software was used to draw a line from the basal side of CMs to the endocardium.

Circularity of CMs

Circularity of compact layer cardiomyocytes in the outer curvature of the ventricle at the mid-sagittal plane was measured using ImageJ as described previously (Rasouli and Stainier, 2017).

Percentage of depolarized CMs in *crb2a*$^{-/-}$

Confocal images (mid-sagittal ventricular plane) were used to count the number of polarized and depolarized CMs in the outer curvature of *crb2a*$^{+/+}$ and *crb2a*$^{-/-}$ hearts using the ZEN software.

In vivo imaging of stopped zebrafish hearts

Embryos and larvae were mounted in 1% low melt agarose in glass-bottomed dishes. In order to stop the heart beat before imaging, 0.2% (w/v) tricaine was added to the agarose. *Z*-plane images were taken using a spinning disc confocal microscope (Zeiss, CSU-X1 Yokogawa), an LSM800 or an LSM880 (Zeiss). A 40× [1.1 numerical aperture (NA)] water-immersion objective was used to acquire the images. The optical sections were 1 µm thick.

Image processing and analysis

Three-dimensional images were processed using the Imaris ×64 (Bitplane, 7.9.0) software. To quantify the number of CMs in the trabecular versus compact layer, the ZEN software was used. The Fiji or ZEN software was used for the rest of the 2D image processing. Images and schemes were prepared using Adobe Photoshop and PowerPoint.

Statistical analysis

Data are expressed as mean±s.e.m. Differences between groups were compared using a two-tailed Student's t distribution test or ANOVA. All tests were performed with a confidence level of 95% (*P<0.05; **P<0.01; ***P<0.001; ****P<0.0001; ns, no significant changes observed).

Acknowledgements

We thank Xiangyun Wei and Chuanyu Guo (University of Pittsburgh, PA, USA) for sharing the Crb2a antibody; Elizabeth Knüst and Cátia Crespo for providing the *crb2a* mutant and the genotyping protocol; Rubén Marín-Juez, Rashmi Priya, Jason Lai, Felix Gunawan, Sophie Ramas, Chi-Chung Wu and Sally Horne-Badovinac for helpful discussions and sharing reagents and expertise; Rubén Marín-Juez, Rashmi Priya and Michelle Collins for critical reading of the manuscript and feedback; Hans-Martin Maischein and Simon Howard for help with zebrafish transplantations and injections; Felix Gunawan for the immunostaining protocol; and Rita Retzloff, Martin Laszczyk and their teams for zebrafish care. V.J.-A. is a graduate student registered with the Faculty of Biological Sciences at Goethe University, Frankfurt am Main, Germany. Some data from this manuscript form part of V.J.-A.'s PhD thesis entitled 'Cardiomyocyte apicobasal polarity during cardiac trabeculation in zebrafish', which was submitted to Goethe University, Frankfurt am Main, Germany, in June 2018.

Competing interests

The authors declare no competing or financial interests.

Author contributions

Conceptualization: V.J.-A., D.Y.R.S.; Methodology: V.J.-A., D.Y.R.S.; Validation: V.J.-A.; Formal analysis: V.J.-A.; Investigation: V.J.-A.; Resources: D.Y.R.S.; Writing - original draft: V.J.-A., D.Y.R.S.; Writing - review & editing: V.J.-A., D.Y.R.S.; Visualization: V.J.-A., D.Y.R.S.; Supervision: D.Y.R.S.; Project administration: D.Y.R.S.; Funding acquisition: D.Y.R.S.

Funding

These studies were supported by funds from the Max-Planck-Gesellschaft.

Supplementary information

Supplementary information available online at http://dev.biologists.org/lookup/doi/10.1242/dev.171207.supplemental

References

Alves, C. H., Sanz Sanz, A., Park, B., Pellissier, L. P., Tanimoto, N., Beck, S. C., Huber, G., Murtaza, M., Richard, F., Sridevi Gurubaran, I. et al. (2013). Loss of *CRB2* in the mouse retina mimics human retinitis pigmentosa due to mutations in the *CRB1* gene. *Hum. Mol. Genet.* **22**, 35-50. doi:10.1093/hmg/dds398

Bilder, D., Li, M. and Perrimon, N. (2000). Cooperative regulation of cell polarity and growth by *Drosophila* tumor suppressors. *Science* **289**, 113. doi:10.1126/science.289.5476.113

Bulgakova, N. A. and Knüst, E. (2009). The Crumbs complex: from epithelial-cell polarity to retinal degeneration. *J. Cell Sci.* **122**, 2587. doi:10.1242/jcs.023648

Chen, C. L., Gajewski, K. M., Hamaratoglu, F., Bossuyt, W., Sansores-Garcia, L., Tao, C. and Halder, G. (2010). The apical-basal cell polarity determinant *Crumbs* regulates Hippo signaling in *Drosophila*. *Proc. Nalt. Acad. Sci. USA* **107**, 15810-15815. doi:10.1073/pnas.1004060107

Cherian, A. V., Fukuda, R., Augustine, S. M., Maischein, H.-M. and Stainier, D. Y. R. (2016). N-cadherin relocalization during cardiac trabeculation. *Proc. Nalt. Acad. Sci. USA* **113**, 7569-7574. doi:10.1073/pnas.1606385113

Costa, M., Raich, W., Agbunag, C., Leung, B., Hardin, J. and Priess, J. R. (1998). A putative catenin–cadherin system mediates morphogenesis of the *Caenorhabditis elegans* mmbryo. *J. Cell Biol.* **141**, 297-308. doi:10.1083/jcb.141.1.297

D'Amico, L., Scott, I. C., Jungblut, B. and Stainier, D. Y. R. (2007). A mutation in zebrafish *hmgcr1b* reveals a role for isoprenoids in vertebrate heart-tube formation. *Curr. Biol.* **17**, 252-259. doi:10.1016/j.cub.2006.12.023

Das, S. and Knüst, E. (2018). A dual role of the extracellular domain of *Drosophila* Crumbs for morphogenesis of the embryonic neuroectoderm. *Biol. Open* **7**, bio031435. doi:10.1242/bio.031435

Etienne-Manneville, S. (2013). Microtubules in cell migration. *Annu. Rev. Cell Dev. Biol.* **29**, 471-499. doi:10.1146/annurev-cellbio-101011-155711

Fan, S.-S., Chen, M.-S., Lin, J.-F., Chao, W.-T. and Yang, V.-C. (2003). Use of gain-of-function study to delineate the roles of *crumbs* in *Drosophila* eye development. *J. Biomed. Sci.* **10**, 766-773. doi:10.1159/000073964

Flores-Benitez, D. and Knüst, E. (2015). *Crumbs* is an essential regulator of cytoskeletal dynamics and cell-cell adhesion during dorsal closure in *Drosophila*. *eLife* **4**, e07398. doi:10.7554/eLife.07398

Gassmann, M., Casagranda, F., Orioli, D., Simon, H., Lai, C., Klein, R. and Lemke, G. (1995). Aberrant neural and cardiac development in mice lacking the ErbB4 neuregulin receptor. *Nature* **378**, 390. doi:10.1038/378390a0

Gorfinkiel, N. (2013). Mechano-chemical coupling drives cell area oscillations during morphogenesis. *Biophys. J.* **104**, 1-3. doi:10.1016/j.bpj.2012.11.3822

Grawe, F., Wodarz, A., Lee, B., Knüst, E. and Skaer, H. (1996). The *Drosophila* genes *crumbs* and *stardust* are involved in the biogenesis of adherens junctions. *Development* **122**, 951.

Grifoni, D., Froldi, F. and Pession, A. (2013). Connecting epithelial polarity, proliferation and cancer in *Drosophila*: the many faces of lgl loss of function. *Int. J. Dev. Biol.* **57**, 677-687. doi:10.1387/ijdb.130285dg

Heisenberg, C.-P. and Bellaïche, Y. (2013). Forces in tissue morphogenesis and patterning. *Cell* **153**, 948-962. doi:10.1016/j.cell.2013.05.008

Hurd, T. W., Gao, L., Roh, M. H., Macara, I. G. and Margolis, B. (2003). Direct interaction of two polarity complexes implicated in epithelial tight junction assembly. *Nat. Cell Biol.* **5**, 137. doi:10.1038/ncb923

Izaddoost, S., Nam, S.-C., Bhat, M. A., Bellen, H. J. and Choi, K.-W. (2002). *Drosophila Crumbs* is a positional cue in photoreceptor adherens junctions and rhabdomeres. *Nature* **416**, 178. doi:10.1038/nature720

Jaron, R., Rosenfeld, N., Zahdeh, F., Carmi, S., Beni-Adani, L., Doviner, V., Picard, E., Segel, R., Zeligson, S., Carmel, L. et al. (2016). Expanding the phenotype of *CRB2* mutations–A new ciliopathy syndrome? *Clin. Genet.* **90**, 540-544. doi:10.1111/cge.12764

Jenni, R., Rojas, J. and Oechslin, E. (1999). Isolated noncompaction of the myocardium. *N. Engl. J. Med.* **340**, 966-967. doi:10.1056/NEJM199903253401215

Jiménez-Amilburu, V., Rasouli, S. J., Staudt, D. W., Nakajima, H., Chiba, A., Mochizuki, N. and Stainier, D. Y. R. (2016). In Vivo visualization of cardiomyocyte apicobasal polarity reveals epithelial to mesenchymal-like transition during cardiac trabeculation. *Cell Rep.* **17**, 2687-2699. doi:10.1016/j.celrep.2016.11.023

Jin, S. W., Beis, D., Mitchell, T., Chen, J. N. and Stainier, D. Y. R. (2005). Cellular and molecular analyses of vascular tube and lumen formation in zebrafish. *Development* **132**, 5199. doi:10.1242/dev.02087

Kemphues, K. J., Priess, J. R., Morton, D. G. and Cheng, N. (1988). Identification of genes required for cytoplasmic localization in early *C. elegans* embryos. *Cell* **52**, 311-320. doi:10.1016/S0092-8674(88)80024-2

Kempkens, Ö., Médina, E., Fernandez-Ballester, G., Özüyaman, S., Le Bivic, A., Serrano, L. and Knüst, E. (2006). Computer modelling in combination with in vitro studies reveals similar binding affinities of *Drosophila Crumbs* for the PDZ domains of *Stardust* and *DmPar*-6. *Eur. J. Cell Biol.* **85**, 753-767. doi:10.1016/j.ejcb.2006.03.003

Lai, J. K. H., Collins, M. M., Uribe, V., Jiménez-Amilburu, V., Günther, S., Maischein, H.-M. and Stainier, D. Y. R. (2018). The Hippo pathway effector *Wwtr1* regulates cardiac wall maturation in zebrafish. *Development* **145**, dev159210. doi:10.1242/dev.159210

Lecuit, T. and Yap, A. S. (2015). E-cadherin junctions as active mechanical integrators in tissue dynamics. *Nat. Cell Biol.* **17**, 533-539. doi:10.1038/ncb3136

Lecuit, T., Lenne, P. F. and Munro, E. (2011). Force generation, transmission, and integration during cell and tissue morphogenesis. *Annu. Rev. Cell Dev. Biol.* **27**, 157-184. doi:10.1146/annurev-cellbio-100109-104027

Lee, K.-F., Simon, H., Chen, H., Bates, B., Hung, M.-C. and Hauser, C. (1995). Requirement for neuregulin receptor erbB2 in neural and cardiac development. *Nature* **378**, 394. doi:10.1038/378394a0

Lee, J., Fei, P., Packard, R. R. S., Kang, H., Xu, H., Baek, K. I., Jen, N., Chen, J., Yen, H., Kuo, C.-C. J. et al. (2016). 4-Dimensional light-sheet microscopy to elucidate shear stress modulation of cardiac trabeculation. *J. Clin. Invest.* **126**, 1679-1690. doi:10.1172/JCI83496

Letizia, A., Ricardo, S., Moussian, B., Martín, N. and Llimargas, M. (2013). A functional role of the extracellular domain of *Crumbs* in cell architecture and apicobasal polarity. *J. Cell Sci.* **126**, 2157-2163. doi:10.1242/jcs.122382

Li, J., Miao, L., Shieh, D., Spiotto, E., Li, J., Zhou, B., Paul, A., Schwartz, R. J., Firulli, A. B., Singer, H. A. et al. (2016). Single cell lineage tracing reveals that oriented cell division contributes to trabecular morphogenesis and regional specification. *Cell Rep.* **15**, 158-170. doi:10.1016/j.celrep.2016.03.012

Lin, Y. F., Swinburne, I. and Yelon, D. (2012). Multiple influences of blood flow on cardiomyocyte hypertrophy in the embryonic zebrafish heart. *Dev. Biol.* **362**, 242-253. doi:10.1016/j.ydbio.2011.12.005

Liu, J., Bressan, M., Hassel, D., Huisken, J., Staudt, D., Kikuchi, K., Poss, K. D., Mikawa, T. and Stainier, D. Y. R. (2010). A dual role for ErbB2 signaling in cardiac trabeculation. *Development* **137**, 3867-3875. doi:10.1242/dev.053736

Macara, I. G. and McCaffrey, L. (2013). Cell polarity in morphogenesis and metastasis. *Philos. Trans. R. Soc. B Biol. Sci.* **368**, 20130012. doi:10.1098/rstb.2013.0012

Malicki, J., Neuhauss, S. C., Schier, A. F., Solnica-Krezel, L., Stemple, D. L., Stainier, D. Y., Abdelilah, S., Zwartkruis, F., Rangini, Z. and Driever, W. (1996). Mutations affecting development of the zebrafish retina. *Development* **123**, 263.

Martin-Belmonte, F. and Mostov, K. (2008). Regulation of cell polarity during epithelial morphogenesis. *Curr. Opin. Cell Biol.* **20**, 227-234. doi:10.1016/j.ceb.2008.01.001

Martin, A. C., Gelbart, M., Fernandez-Gonzalez, R., Kaschube, M. and Wieschaus, E. F. (2010). Integration of contractile forces during tissue invagination. *J. Cell Biol.* **188**, 735. doi:10.1083/jcb.200910099

Meyer, D. and Birchmeier, C. (1995). Multiple essential functions of neuregulin in development. *Nature* **378**, 386. doi:10.1038/378386a0

Omori, Y. and Malicki, J. (2006). *oko meduzy* and related *crumbs* genes are determinants of apical cell features in the vertebrate embryo. *Curr. Biol.* **16**, 945-957. doi:10.1016/j.cub.2006.03.058

Passer, D., van de Vrugt, A., Atmanli, A. and Domian, I. (2016). Atypical protein kinase C dependent polarized cell division is required for myocardial trabeculation. *Cell Rep.* **14**, 1662-1672. doi:10.1016/j.celrep.2016.01.030

Pénalva, C. and Mirouse, V. (2012). Tissue-specific function of *Patj* in regulating the Crumbs complex and epithelial polarity. *Development* **139**, 4549. doi:10.1242/dev.085449

Peshkovsky, C., Totong, R. and Yelon, D. (2011). Dependence of cardiac trabeculation on neuregulin signaling and blood flow in zebrafish. *Dev. Dyn.* **240**, 446-456. doi:10.1002/dvdy.22526

Raich, W. B., Agbunag, C. and Hardin, J. (1999). Rapid epithelial-sheet sealing in the Caenorhabditis elegans embryo requires cadherin-dependent filopodial priming. *Curr. Biol.* **9**, S1139-S1131. doi:10.1016/S0960-9822(00)80015-9

Rasouli, S. J. and Stainier, D. Y. R. (2017). Regulation of cardiomyocyte behavior in zebrafish trabeculation by Neuregulin 2a signaling. *Nat. Commun.* **8**, 15281. doi:10.1038/ncomms15281

Revenu, C., Streichan, S., Donà, E., Lecaudey, V., Hufnagel, L. and Gilmour, D. (2014). Quantitative cell polarity imaging defines leader-to-follower transitions during collective migration and the key role of microtubule-dependent adherens junction formation. *Development* **141**, 1282. doi:10.1242/dev.101675

Rottbauer, W., Saurin, A. J., Lickert, H., Shen, X., Burns, C. G., Wo, Z. G., Kemler, R., Kingston, R., Wu, C. and Fishman, M. (2002). *Reptin* and *Pontin* antagonistically regulate heart growth in zebrafish embryos. *Cell* **111**, 661-672. doi:10.1016/S0092-8674(02)01112-1

Samsa, L. A., Yang, B. and Liu, J. (2013). Embryonic cardiac chamber maturation: Trabeculation, conduction and cardiomyocyte proliferation. *Am. J. Med. Genet. C Semin. Med. Genet.* **163**, 157-168. doi:10.1002/ajmg.c.31366

Samsa, L. A., Givens, C., Tzima, E., Stainier, D. Y. R., Qian, L. and Liu, J. (2015). Cardiac contraction activates endocardial Notch signaling to modulate chamber maturation in zebrafish. *Development* **142**, 4080-4091. doi:10.1242/dev.125724

Sedmera, D., Pexieder, T., Vuillemin, M., Thompson Robert, P. and Anderson Robert, H. (2000). Developmental patterning of the myocardium. *Anat. Rec.* **258**, 319-337. doi:10.1002/(SICI)1097-0185(20000401)258:4<319::AID-AR1>3.0.CO;2-O

Sehnert, A. J., Huq, A., Weinstein, B. M., Walker, C., Fishman, M. and Stainier, D. Y. R. (2002). Cardiac troponin T is essential in sarcomere assembly and cardiac contractility. *Nat. Genet.* **31**, 106. doi:10.1038/ng875

Sherrard, K. M. and Fehon, R. G. (2015). The transmembrane protein Crumbs displays complex dynamics during follicular morphogenesis and is regulated competitively by *Moesin* and *aPKC*. *Development* **142**, 1869. doi:10.1242/dev.115329

Slavotinek, A., Kaylor, J., Pierce, H., Cahr, M., DeWard, S. J., Schneidman-Duhovny,D., Alsadah, A., Salem, F., Schmajuk, G. and Mehta, L. (2015). *CRB2* mutations produce a phenotype resembling congenital nephrosis, Finnish type, with cerebral ventriculomegaly and raised alpha-fetoprotein. *Am. J. Hum. Genet.* **96**, 162-169. doi:10.1016/j.ajhg.2014.11.013

Staudt, D. W., Liu, J., Thorn, K. S., Stuurman, N., Liebling, M. and Stainier, D. Y. R. (2014). High-resolution imaging of cardiomyocyte behavior reveals two distinct steps in ventricular trabeculation. *Development* **141**, 585-593. doi:10.1242/dev.098632

Tanentzapf, G., Smith, C., McGlade, J. and Tepass, U. (2000). Apical, lateral, and basal polarization cues contribute to the development of the follicular epithelium during *Drosophila* oogenesis. *J. Cell Biol.* **151**, 891. doi:10.1083/jcb.151.4.891

Tepass, U. (1996). *Crumbs*, a Component of the apical membrane, is required for zonula adherens formation in primary epithelia of *Drosophila*. *Dev. Biol.* **177**, 217-225. doi:10.1006/dbio.1996.0157

Tepass, U. and Knüst, E. (1990). Phenotypic and developmental analysis of mutations at the crumbs locus, a gene required for the development of epithelia in *Drosophila melanogaster*. *Roux. Arch. Dev. Biol.* **199**, 189-206. doi:10.1007/BF01682078

Uribe, V., Ramadass, R., Dogra, D., Rasouli, S. J., Gunawan, F., Nakajima, H., Chiba, A., Reischauer, S., Mochizuki, N. and Stainier, D. Y. R. (2018). In vivo analysis of cardiomyocyte proliferation during trabeculation. *Development* **145**, dev164194. doi:10.1242/dev.164194

van de Pavert, S. A., Kantardzhieva, A., Malysheva, A., Meuleman, J., Versteeg, I., Levelt, C., Klooster, J., Geiger, S., Seeliger, M. W., Rashbass, P. et al. (2004). *Crumbs homologue* 1 is required for maintenance of photoreceptor cell polarization and adhesion during light exposure. *J. Cell Sci.* **117**, 4169. doi:10.1242/jcs.01301

Weiford, B. C., Subbarao, V. D. and Mulhern, K. M. (2004). Noncompaction of the ventricular myocardium. *Circulation* **109**, 2965-2971. doi:10.1161/01.CIR.0000132478.60674.D0

Wu, Y., Sarkissyan, M. and Vadgama, J. V. (2016). Epithelial-Mesenchymal Transition and breast cancer. *J. Clin. Med.* **5**, 13. doi:10.3390/jcm5020013

Xiao, Z., Patrakka, J., Nukui, M., Chi, L., Niu, D., Betsholtz, C., Pikkarainen, T., Vainio, S. and Tryggvason, K. (2011). Deficiency in *crumbs homolog 2 (Crb2)* affects gastrulation and results in embryonic lethality in mice. *Dev. Dyn.* **240**, 2646-2656. doi:10.1002/dvdy.22778

Xu, N., Keung, B. and Myat, M. M. (2008). Rho GTPase controls invagination and cohesive migration of the *Drosophila* salivary gland through *Crumbs* and Rho-kinase. *Dev. Biol.* **321**, 88-100. doi:10.1016/j.ydbio.2008.06.007

Zhang, W., Chen, H., Qu, X., Chang, C.-P. and Shou, W. (2013). Molecular mechanism of ventricular trabeculation/compaction and the pathogenesis of the left ventricular noncompaction cardiomyopathy (LVNC). *Am. J. Med. Genet. C Semin. Med. Genet.* **163**, 144-156. doi:10.1002/ajmg.c.31369

Zou, J., Wang, X. and Wei, X. (2012). Crb apical polarity proteins maintain zebrafish retinal cone mosaics via intercellular binding of their extracellular domains. *Dev. Cell* **22**, 1261-1274. doi:10.1016/j.devcel.2012.03.007

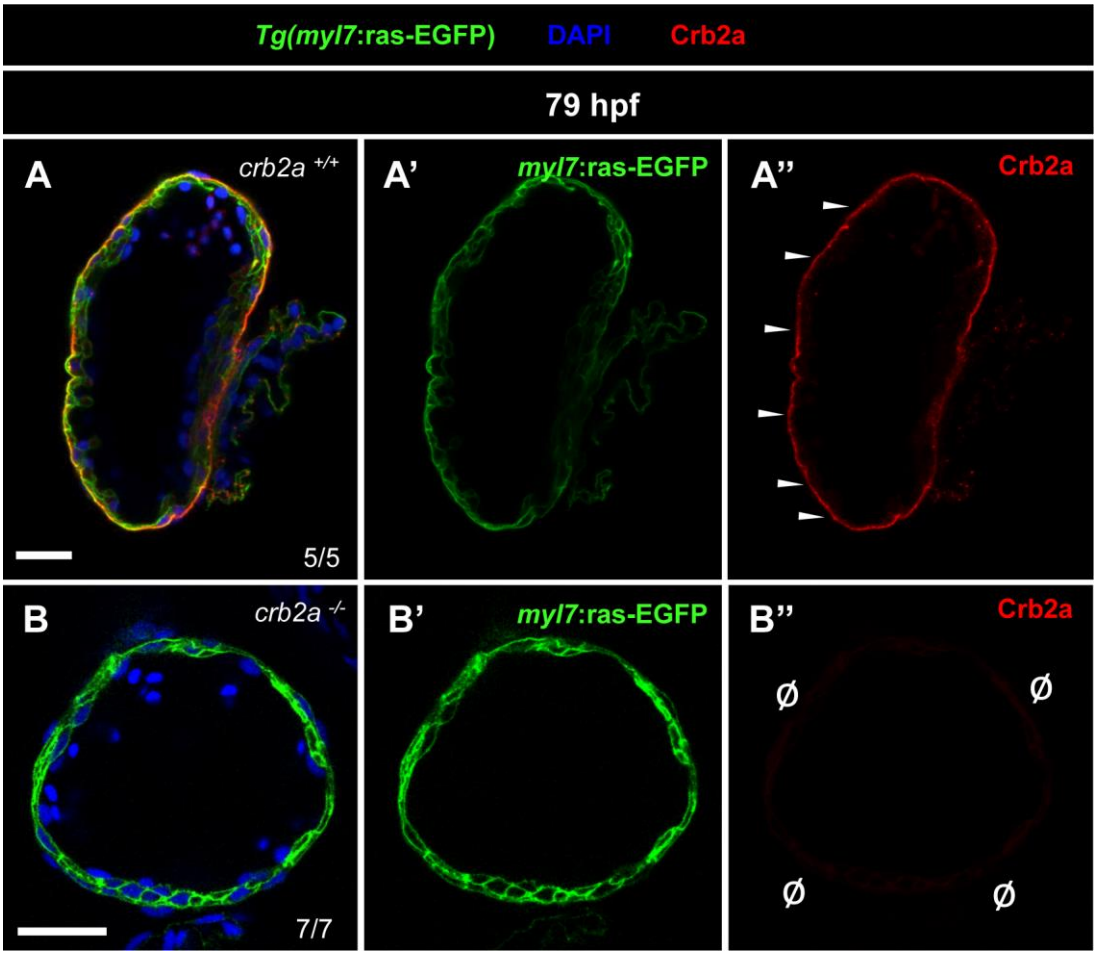

Figure S1. Lack of Crb2a staining in *crb2a* mutant hearts.

(A-B'') Crb2a immunostaining in 79 hpf *Tg(myl7:ras-EGFP) crb2a*$^{+/+}$ (A-A'') and *crb2a*$^{-/-}$ (B-B'') hearts. White arrowheads point to apical localization of Crb2a in *crb2a*$^{+/+}$ compact layer CMs (A''), while ø indicates lack of Crb2a immunostaining in *crb2a*$^{-/-}$ hearts (B''). V, ventricle. Scale bars, 20 μm.

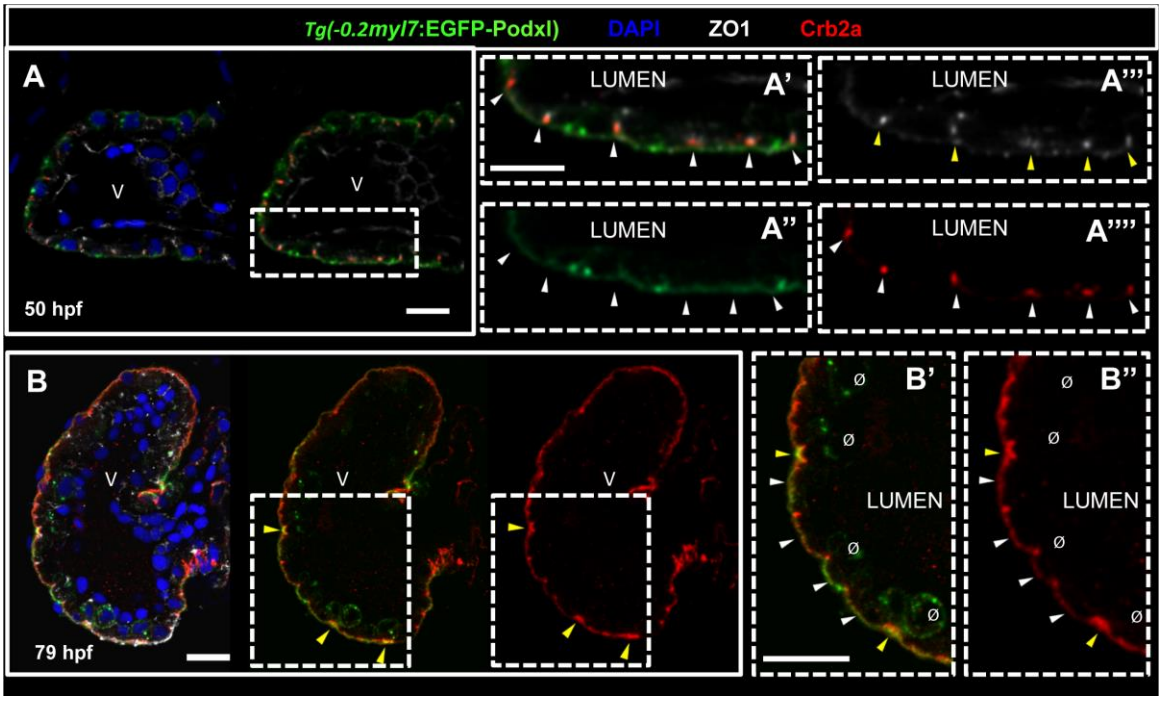

Figure S2. Crb2a co-localizes with ZO-1 in early CMs and subsequently with Podocalyxin.

(A-B'') Crb2a immunostaining in *Tg(−0.2myl7:EGFP-podxl)* hearts at 50 (A-A'''') and 79 (B-B'') hpf. At 50 hpf, Crb2a localizes to the junctions between CMs at the apical side, coinciding with ZO-1 immunostaining (A'-A'''', arrowheads). At 79 hpf, some compact layer CMs are undergoing apical constriction (B, yellow arrowheads), and Crb2a accumulates at these constricting apical membranes, coinciding with Podocalyxin localization (B'-B'', yellow arrowheads). Moreover, Crb2a expression extends to the apical membrane of compact layer CMs co-localizing with Podocalyxin (B'-B'', white arrowheads). At 79 hpf, Crb2a expression was not observed in delaminated CMs (B'-B'', Ø). V, ventricle. Scale bars, 20 μm.

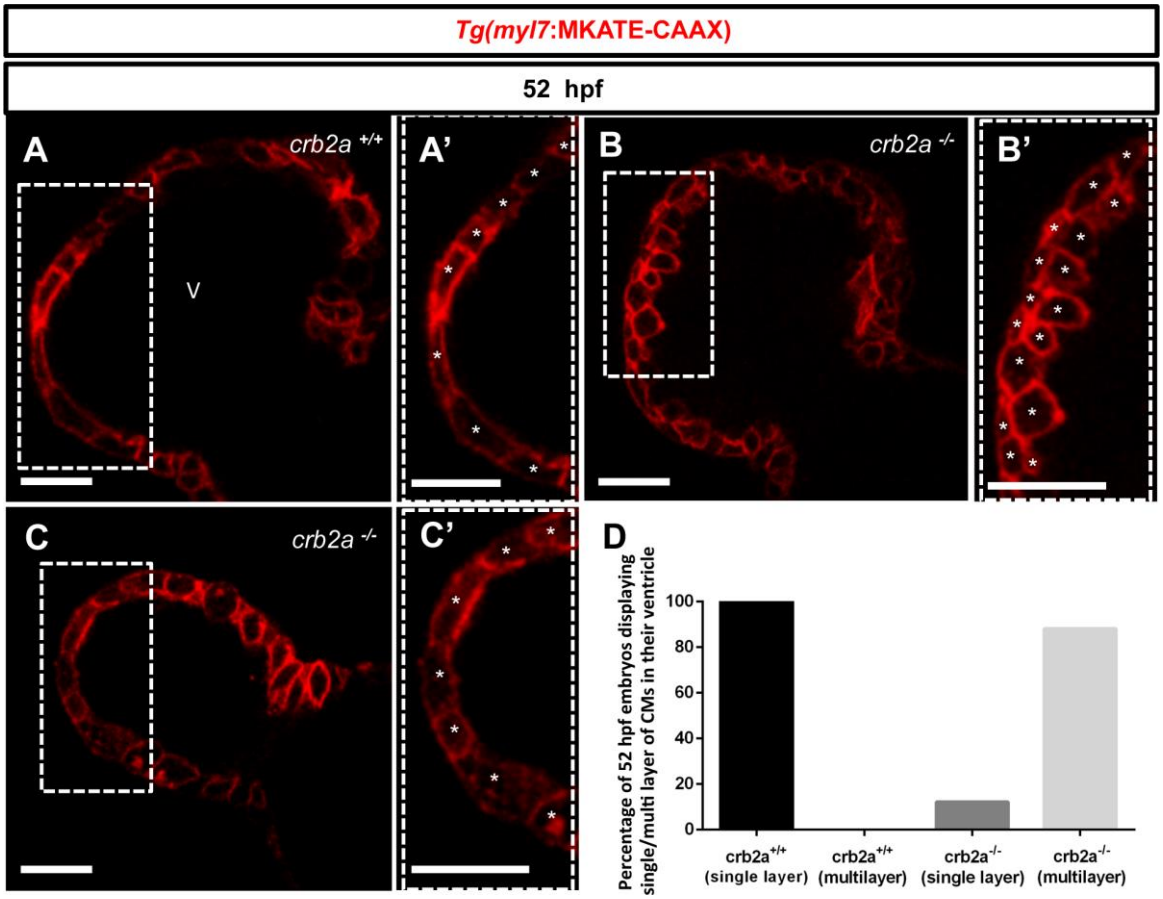

Figure S3. *crb2a*$^{-/-}$ hearts display CM multilayering at 52 hpf

(A-C') Confocal images (mid-sagittal sections) of 52 hpf *Tg(myl7:MKATE-CAAX) crb2a*$^{+/+}$ (A-A', n=8) and *crb2a*$^{-/-}$ (B-C', n=22) hearts. Higher magnification images of *crb2a*$^{+/+}$ hearts show a single layer of CMs in the ventricle (A', asterisks). Higher magnification images show a single layer of CMs in the ventricle of 3/22 mutants analyzed (B', asterisks), while the other 19 display multiple layers of CMs in their ventricle (C', asterisks). (D) Percentage of 52 hpf embryos showing single or multiple CM layers in their ventricle. V, ventricle. Scale bars, 20 μm.

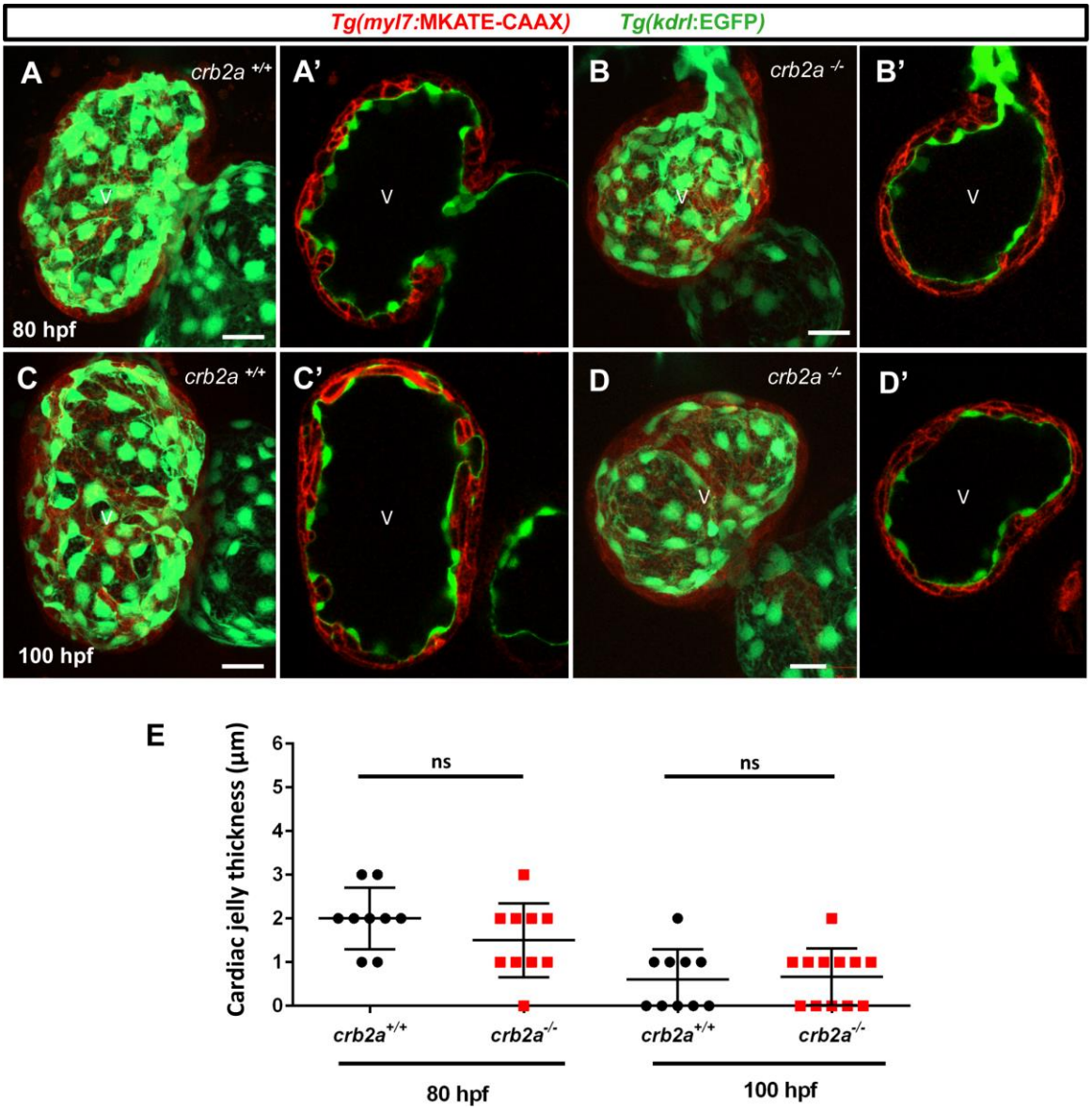

Figure S4. Cardiac jelly reduction is not affected in *crb2a*$^{-/-}$.

(A-D') Confocal images (maximum intensity projections) of *Tg(kdrl:EGFP)*; *Tg(myl7:MKATE-CAAX)* *crb2a*$^{+/+}$ and *crb2a*$^{-/-}$ hearts at 80 (n=9; n=10) and 100 (n=10; n=12) hpf. *crb2a*$^{-/-}$ hearts display a WT-like reduction of the cardiac jelly at both stages. (E) Quantification of cardiac jelly thickness at 80 and 100 hpf. V, ventricle. Scale bars, 20 µm.

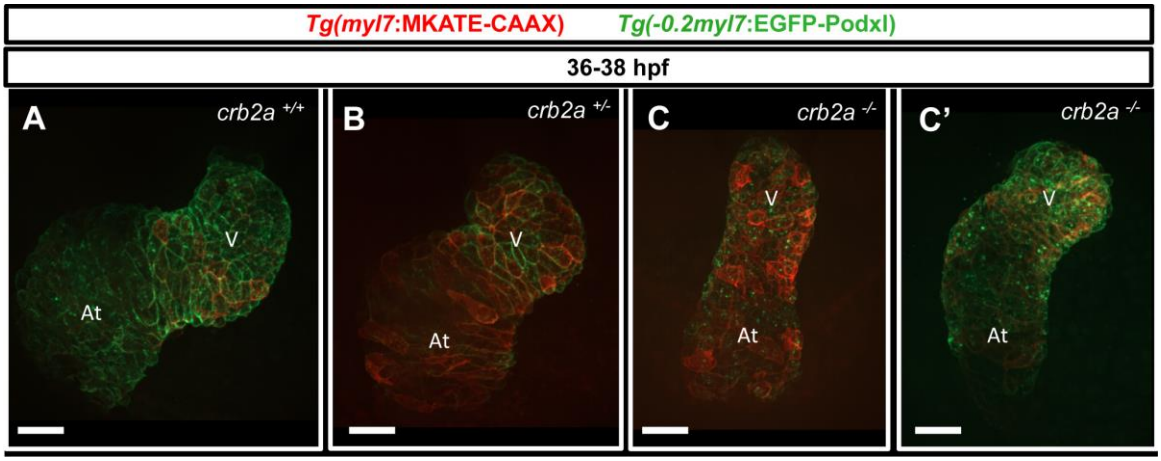

Figure S5. *crb2a* mutant hearts exhibit looping defects.

(A-C') 3D maximum intensity projections of 36-38 hpf *Tg(−0.2myl7:EGFP-podxl)*; *Tg(myl7:MKATE-CAAX)* hearts. Compared to *crb2a*$^{+/+}$ (A (6/6)) and *crb2a*$^{+/-}$ (B (10/11)) hearts, *crb2a*$^{-/-}$ hearts display no looping (C (4/11)) or delayed looping (C' (7/11)). V, ventricle; At, atrium. Scale bars, 20 μm.

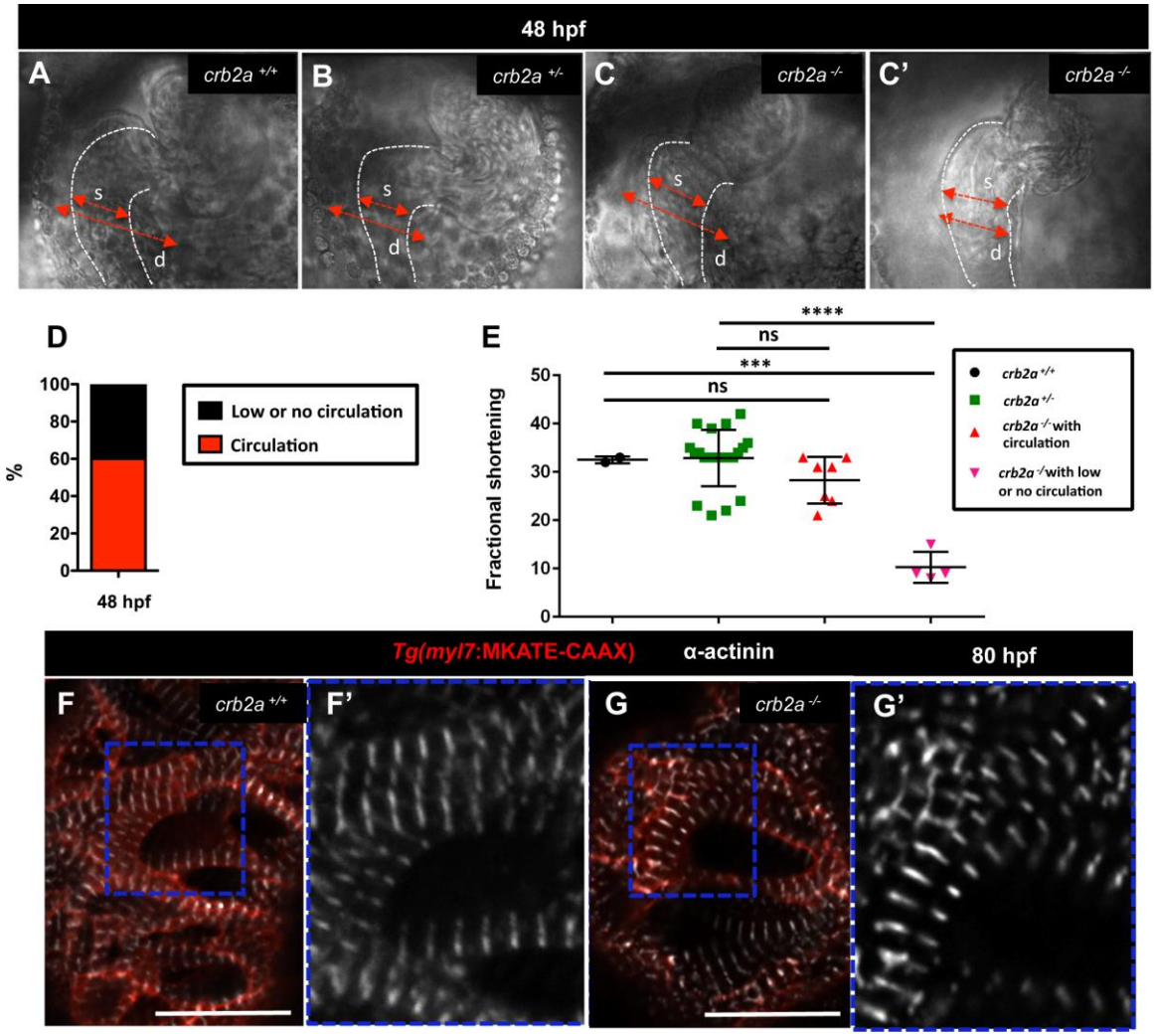

Figure S6. *crb2a*$^{-/-}$ hearts display functional defects at 48 hpf.

(A-C') Brightfield images of 48 hpf hearts. Red arrows indicate length of diastole (d) and systole (s). White dashed lines represent the heart shape in systole. (D) Percentage of mutant embryos with normal, low, or no circulation at 48 hpf. Total number of embryos analyzed: 650; total number of mutants analyzed, 124 (with circulation (n=50), with low or no circulation (n=74)). (E) Fractional shortening of *crb2a*$^{+/+}$, *crb2a*$^{+/-}$ and *crb2a*$^{-/-}$ hearts. One way analysis of variance (ANOVA) was performed corrected by Tukey's multiple comparisons test; $P < 0.001$, $^{****}P < 0.0001$. (F-G') Confocal images of α-actinin immunostaining in 80 hpf *Tg(myl7:MKATE-CAAX)* ventricles. Blue boxes show high magnification images of *crb2a*$^{+/+}$ (F') and *crb2a*$^{-/-}$ (G') hearts. Scale bars, 20 μm.

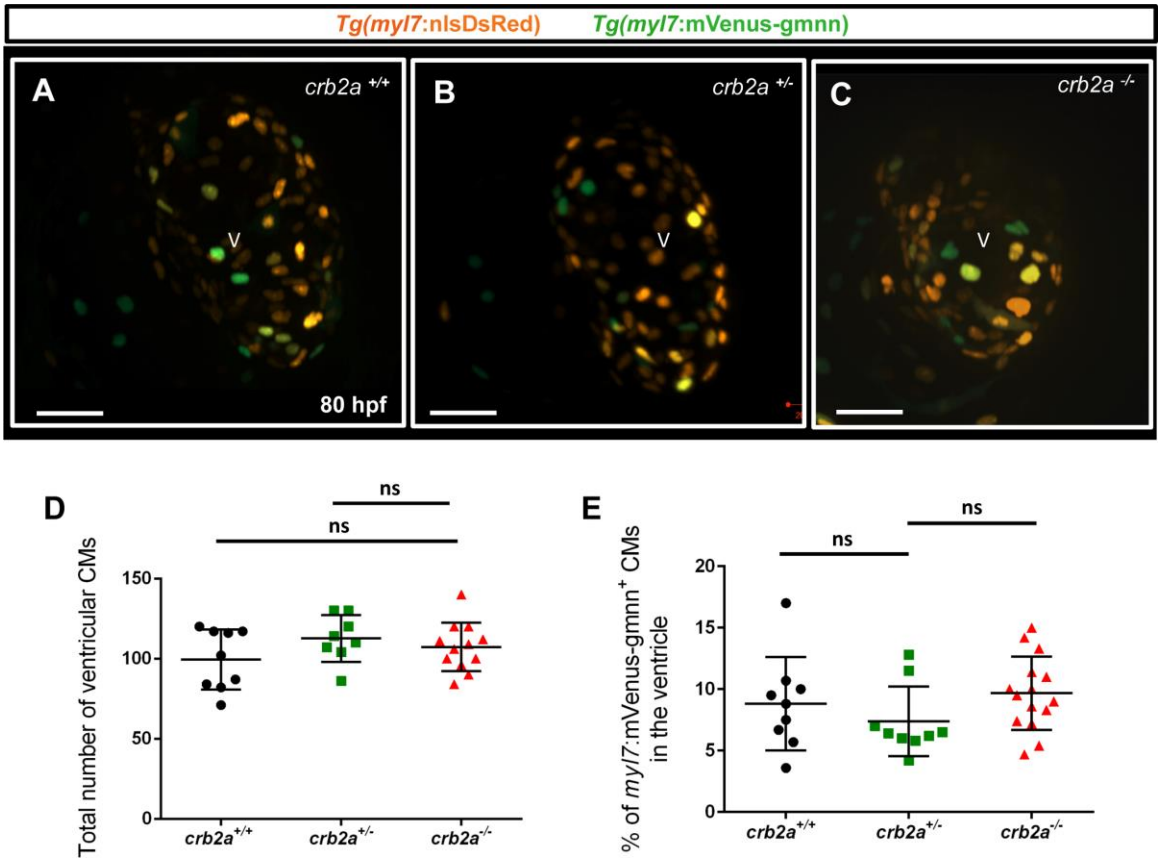

Figure S7. *crb2a*$^{-/-}$ ventricles do not exhibit an increase in CM proliferation.
(A-C) Confocal images (maximum intensity projections) of 80 hpf *Tg(myl7:nlsDsRed); Tg(myl7:mVenus-gmnn)* hearts. (D) Total number of ventricular CMs. (E) Percentage of *myl7*:mVenus-Gmnn^{+} CMs in the ventricle. Each dot represents a heart. One way analysis of variance (ANOVA) was performed corrected by Tukey's multiple comparisons test; ns, no significant differences. V, ventricle. Scale bars, 20 μm.

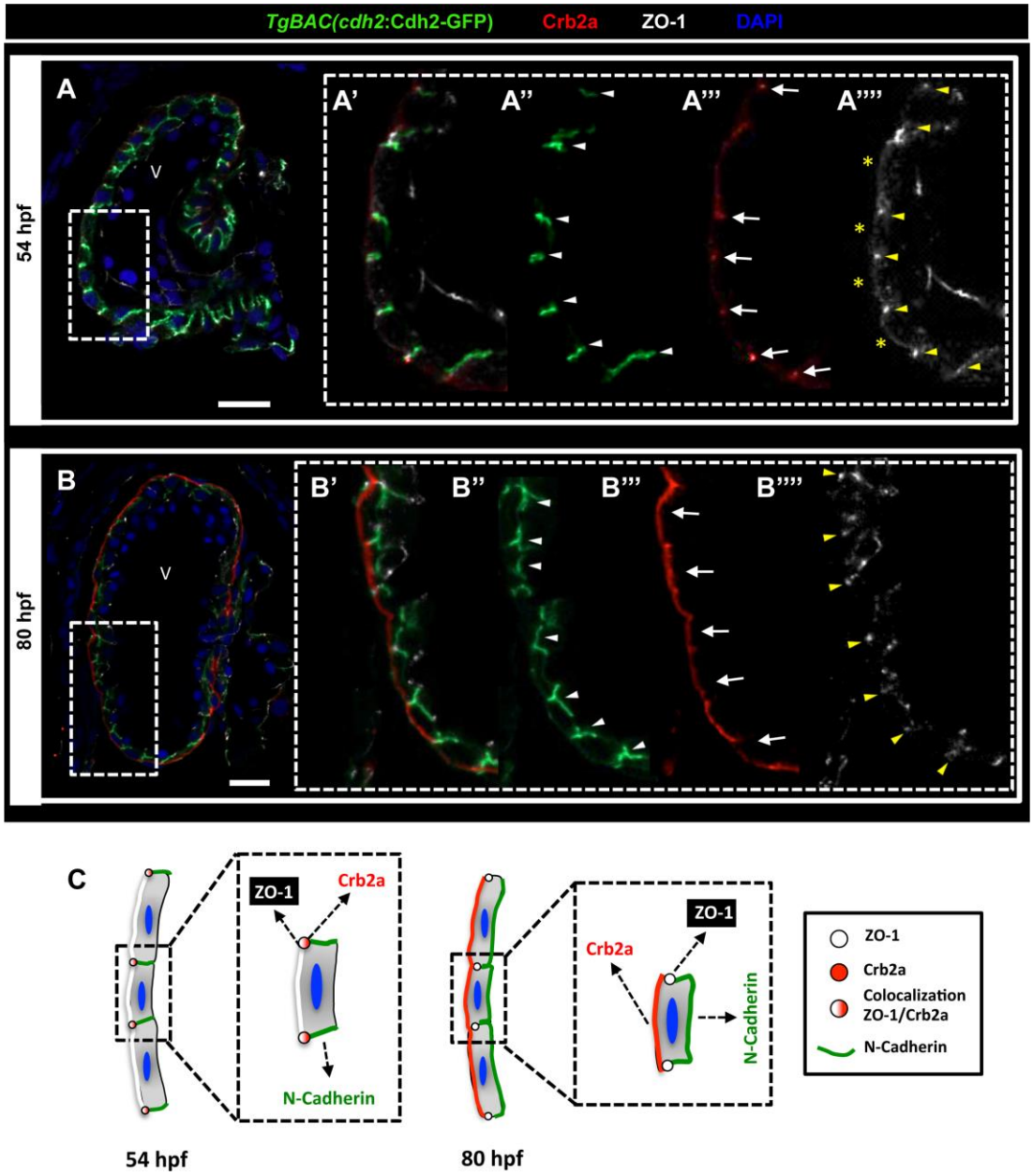

Figure S8. Localization of TJ and AJ proteins and Crb2a in CMs during trabeculation.

(A-B'''') Crb2a and ZO-1 immunostainings in *TgBAC(cdh2:Cdh2-GFP)* hearts at 54 (A-A'''') and 80 (B-B'''') hpf. At 54 hpf, white arrowheads point to lateral localization of N-Cadherin (A''), white arrows point to junctional localization of Crb2a (A'''), and yellow arrowheads and asterisks indicate junctional and apical ZO-1 immunostaining, respectively (A''''). At 80 hpf, white arrowheads point to basolateral localization of N-Cadherin (B''), white arrows point to apical Crb2a localization (B'''). and yellow arrowheads point to junctional ZO-1 immunostaining (B''''). (C) Schematic representation of TJ and AJ proteins in WT CMs. V, ventricle. Scale bars, 20 μm.

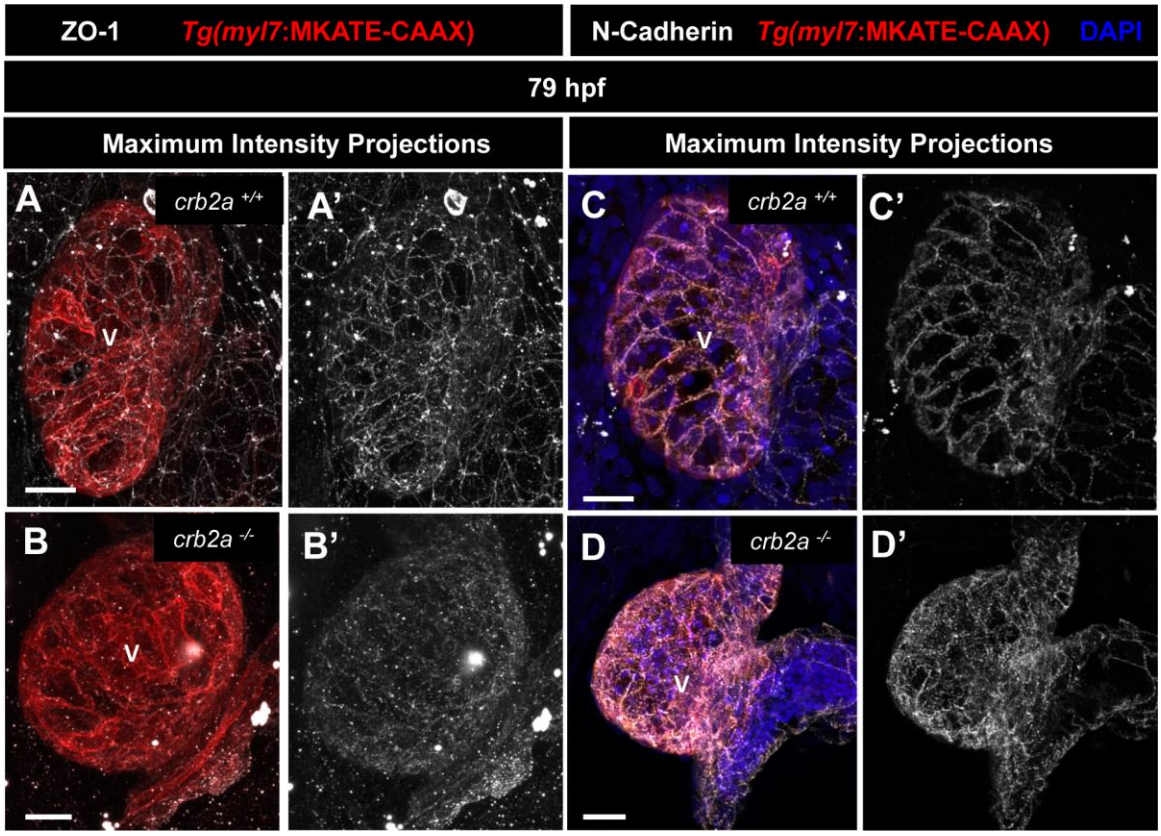

Figure S9. Maximum intensity projection images of TJ and AJ proteins in CMs. (A-B') Maximum intensity projection images of ZO-1 immunostaining in 79 hpf *Tg(myl7:MKATE-CAAX)* hearts show that ZO-1 localizes to the junctions between CMs in *crb2a*$^{+/+}$ (A', n=10), but that its junctional pattern is fragmented in *crb2a*$^{-/-}$ (B', n=16). (C-D') Maximum intensity projection images of N-cadherin immunostaining in 79 hpf *Tg(myl7:MKATE-CAAX)* hearts show that N-Cadherin localizes to the junctions between CMs in *crb2a*$^{+/+}$ embryos (C', n=7), but that it is mislocalized in *crb2a*$^{-/-}$ (D', n=15). V, ventricle. Scale bars, 20 μm.

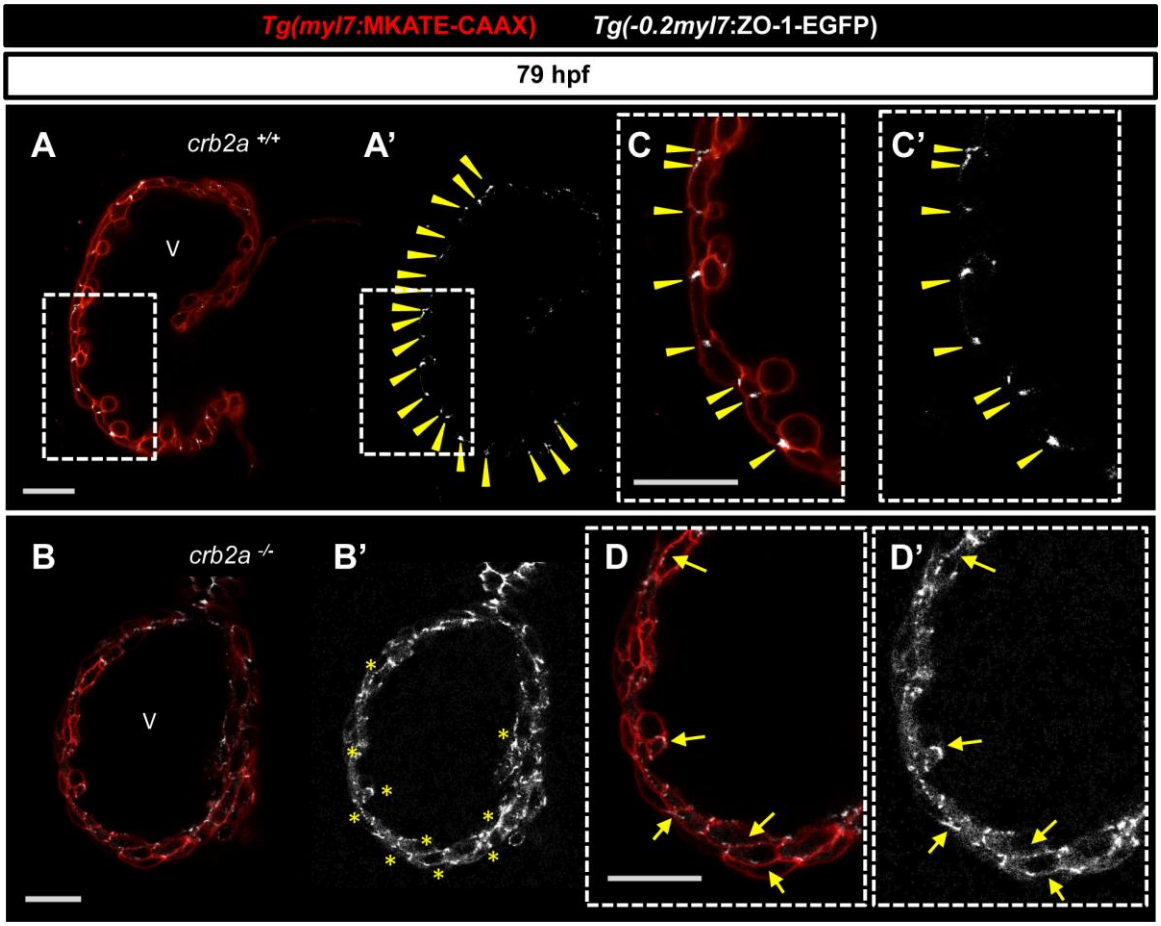

Figure S10. In vivo ZO-1 localization in CMs.

(A-B') Confocal images (mid-sagittal sections) of 79 hpf *Tg(myl7:MKATE-CAAX); Tg(-0.2myl7:ZO-1-EGFP) crb2a*$^{+/+}$ (A-A') and *crb2a*$^{-/-}$ (B-B') hearts; higher magnification images (C-D') show that ZO-1 is present at the junctions between compact layer CMs in *crb2a*$^{+/+}$ (A-A' and C-C', arrrowheads, n= 12), and that it is mislocalized in *crb2a*$^{-/-}$ (B-B' and D-D', arrows, n=11). V, ventricle. Scale bars, 20 μm.

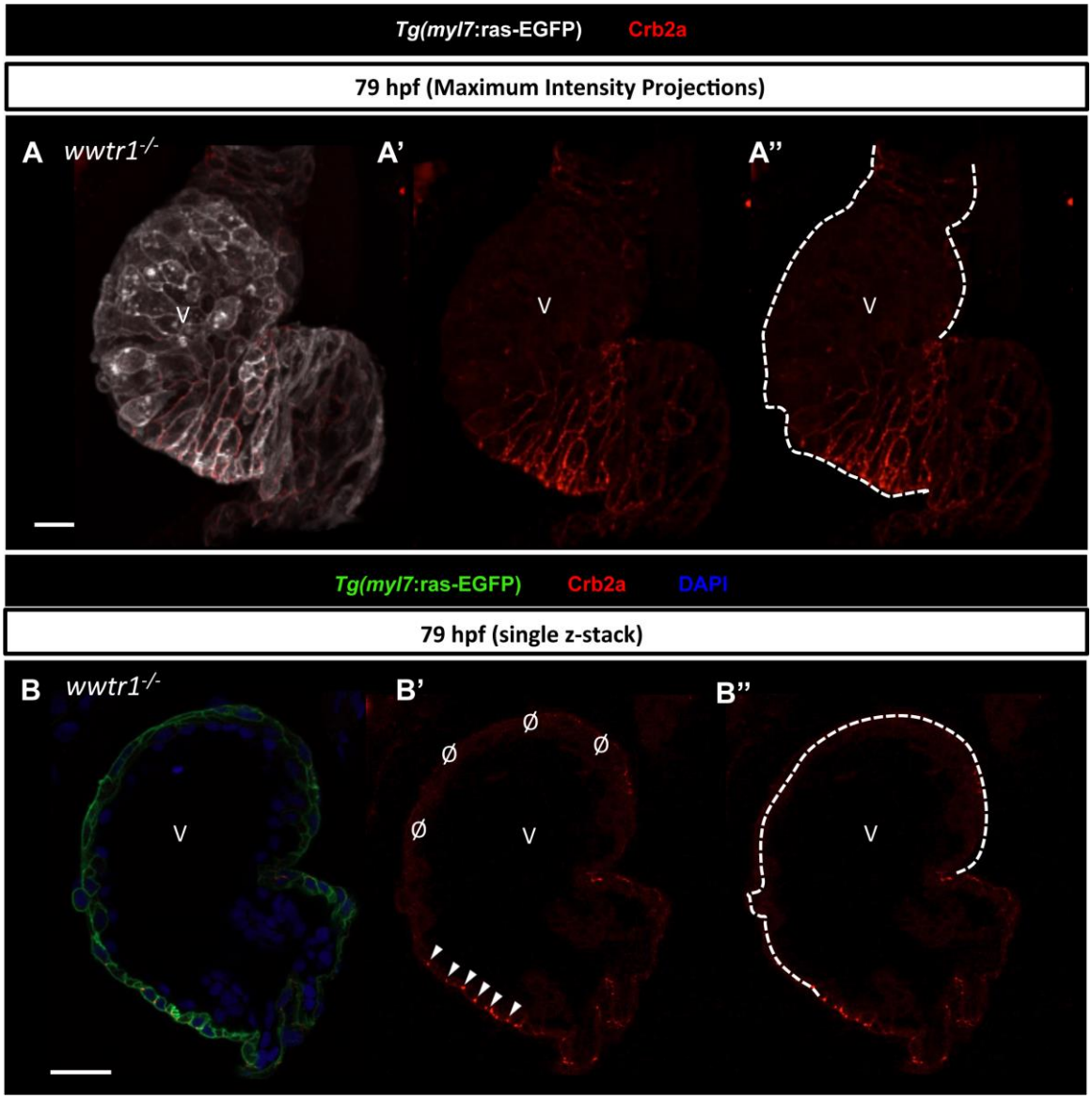

Figure S11. Crb2a expression is lost in *wwtr1*$^{-/-}$ hearts.

(A-A'') Maximum intensity projection images of 79 hpf *Tg(myl7:ras-EGFP) wwtr1*$^{-/-}$ hearts immunostained for Crb2a (n= 7 hearts). (B-B'') Confocal images (mid-sagittal sections) of 79 hpf *Tg(myl7:ras-EGFP) wwtr1*$^{-/-}$ hearts immunostained for Crb2a and DAPI (n=8 hearts). Arrowheads point to junctional Crb2a localization in the outer curvature of the heart, while Ø shows lack of Crb2a immunostaining. White dashed lines outline the compact layer of the ventricle. V, ventricle. Scale bars, 20 μm

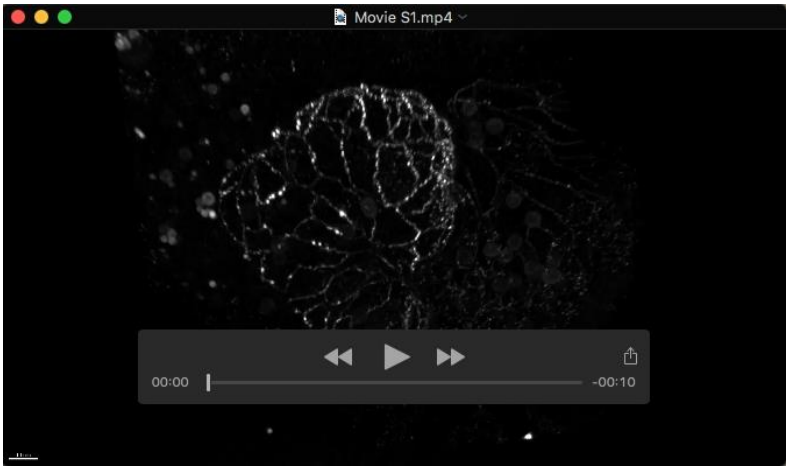

Movie 1. Movie showing Crb2a immunostaining in 3D reconstructed 51 hpf heart.

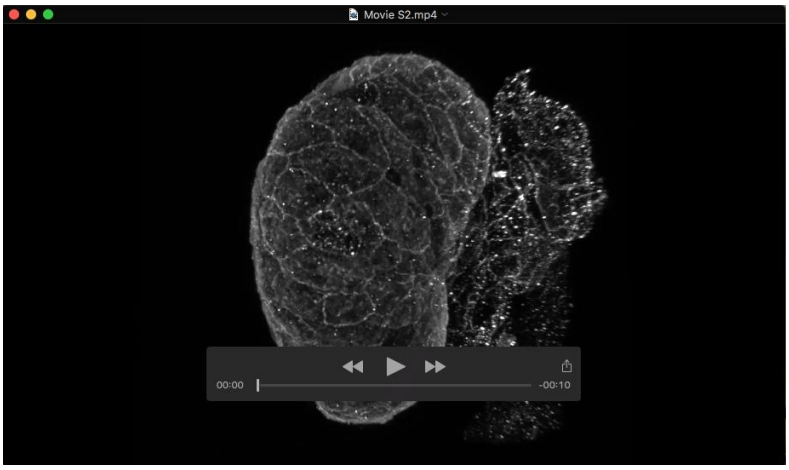

Movie 2. Movie showing Crb2a immunostaining in 3D reconstructed 72 hpf heart.

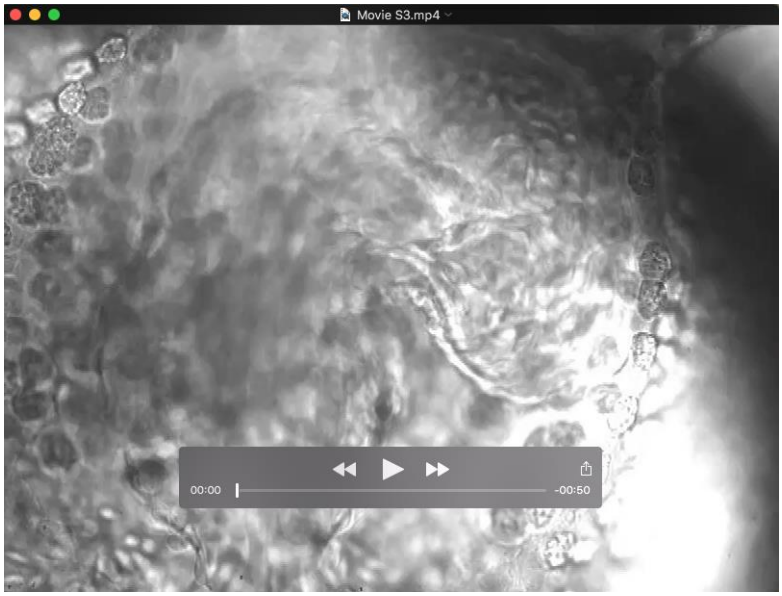

Movie 3. Movie showing beating of 48 hpf *crb2a*$^{+/+}$ zebrafish heart.

Movie 4. Movie showing beating of 48 hpf *crb2a*$^{+/-}$ zebrafish heart.

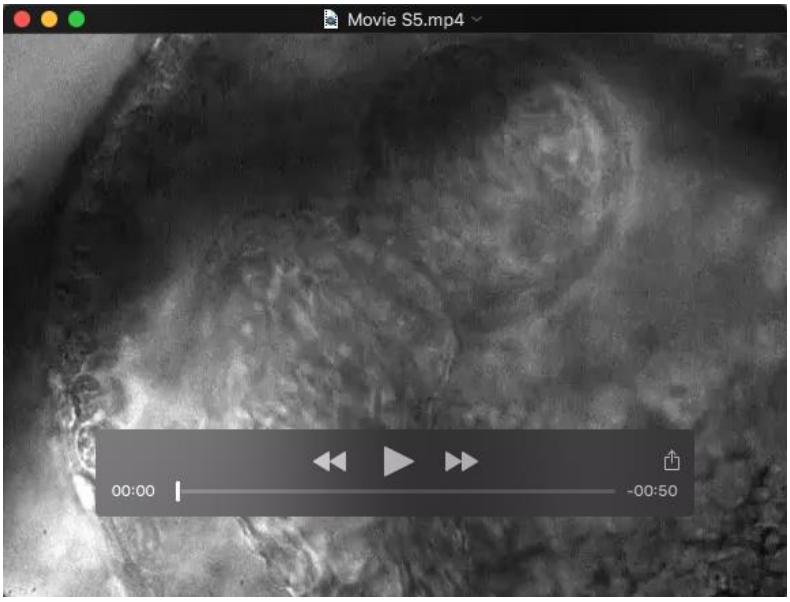

Movie 5. Movie showing beating of 48 hpf *crb2a*$^{-/-}$ zebrafish heart with normal circulation.

Movie 6. Movie showing beating of 48 hpf *crb2a*$^{-/-}$ zebrafish heart with low or no circulation.